ROCS: Robust One-Bit Compressed Sensing with Application to Direction of Arrival

Xiao-Peng Li, *Member, IEEE*, Zhang-Lei Shi, Lei Huang, *Senior Member, IEEE*, Anthony Man-Cho So, *Fellow, IEEE*, Hing Cheung So, *Fellow, IEEE*

Abstract—One-bit compressed sensing (1-bit CS) inherits the merits of traditional CS and further reduces the cost and burden on the hardware device via employing the 1-bit analog-to-digital converter. When the measurements do not involve sign flips caused by additive noise, most contemporary algorithms can attain excellent signal restoration. However, their recovery performance might significantly degrade if there is even a small portion of sign flips. In order to increase the estimation accuracy in noisy scenarios, we devise a new signal model for 1-bit CS to attain robustness against sign flips. Then, we give a double-sparsity optimization formulation of the restoration problem. Subsequently, we combine proximal alternating minimization and projected gradient descent to tackle the problem. Different from existing robust methodologies, our approach, referred to as robust one-bit CS (ROCS), does not require the number of sign flips. Furthermore, we analyze the convergence behavior of ROCS and show that the objective value and variable sequences converge. Numerical results using synthetic data demonstrate that ROCS is superior to the competing methods in terms of reconstruction error in noisy environments. ROCS is also applied to direction-of-arrival estimation and outperforms state-of-the-art approaches.

Index Terms—Robust algorithm, one-bit compressed sensing, direction-of-arrival estimation, ℓ_0-norm optimization.

I. Introduction

TO improve the efficiency of data acquisition, compressed sensing (CS) has been proposed, which adopts the sparsity property to recover a sparse signal from a few measurements [1], [2]. In accordance to the Nyquist-Shannon sampling theorem, a signal must be sampled at least twice as high as its maximum frequency to be perfectly reconstructed. In contrast, CS allows for a lower sampling rate for the

sparse signals. Note that if signals are non-sparse, a linear projection may obtain sparse substitutes. In recent years, the rapid development of data acquisition necessitates collecting a vast quantity of measurements, leading to the challenges in CS, particularly in terms of storage cost and hardware complexity. To handle these issues, one-bit CS (1-bit CS) [3] is suggested via employing 1-bit analog-to-digital converter (ADC) that preserves only the sign information of the measurements. The process of 1-bit quantization can be implemented using a simple comparator to zero, which significantly reduces the cost and burden on hardware devices. Due to this merit, 1-bit CS has been applied in synthetic aperture radar (SAR) imaging [4], [5], direction-of-arrival (DOA) estimation [6], [7], and wireless sensor networks [8], [9], to name a few.

A. Prior Art

Given a sparse signal $\boldsymbol{x} \in \mathbb{R}^N$ with unit energy, its observations after quantization can be expressed as

$$\boldsymbol{y} = \text{sgn}(\boldsymbol{A}\boldsymbol{x}), \qquad (1)$$

where $\text{sgn}(\cdot)$ is the sign function, $\boldsymbol{y} \in \mathbb{R}^M$ and $\boldsymbol{A} \in \mathbb{R}^{M \times N}$ is the measurement matrix with $M < N$. The aim of 1-bit CS is to recover $\boldsymbol{x}$ from $\boldsymbol{y}$ based on $\boldsymbol{A}$. It has been shown that one can recover $\boldsymbol{x}$ from $\boldsymbol{y}$ with high probability if $\boldsymbol{A}$ has the binary ϵ-stable embedding (BϵSE) property [10]. Given a sensing matrix $\boldsymbol{A}$, and two sparse vectors $\boldsymbol{x}_1$ and $\boldsymbol{x}_2$, BϵSE is described as

$$\frac{1}{\pi} \arccos\langle \boldsymbol{x}_1, \boldsymbol{x}_2 \rangle - \epsilon \leq \frac{1}{M} \|\text{sgn}(\boldsymbol{A}\boldsymbol{x}_1) - \text{sgn}(\boldsymbol{A}\boldsymbol{x}_2)\|_0$$
$$\leq \frac{1}{\pi} \arccos\langle \boldsymbol{x}_1, \boldsymbol{x}_2 \rangle + \epsilon, \qquad (2)$$

where $\epsilon \in (0,1)$ and $\|\cdot\|_0$ is ℓ_0-norm corresponding to the number of non-zero entries. For the exact reconstruction guarantee of a sparse signal with a high probability, BϵSE is required in noisy environments but not in noiseless ones [10]. Nonetheless, verifying the BϵSE property for a given matrix may be a computationally intractable task. Instead, $\boldsymbol{A}$ is generally modeled as a Gaussian random matrix.

Based on traditional CS, the ideal optimization model for 1-bit CS is formulated as an ℓ_0-norm minimization problem, subject to two constraints of fitting error and signal energy [11]

$$\min_{\boldsymbol{x}} \|\boldsymbol{x}\|_0 \quad \text{s.t. } \boldsymbol{y} = \text{sgn}(\boldsymbol{A}\boldsymbol{x}), \|\boldsymbol{x}\|_2 = 1. \qquad (3)$$

The energy requirement aims to resolve the amplitude ambiguity as 1-bit quantization cannot retain the signal amplitude information. It is worth noting that non-zero random

quantization threshold has been exploited for signal energy estimation [12]. Besides, one-bit sampling with a dithered reference level is applied for amplitude recovery in [13], [14]. Minimizing ℓ_0-norm is an NP-hard problem [15] and thus ℓ_1-norm is exploited to approximate the ℓ_0-norm for 1-bit CS [3], resulting in

$$\min_{\boldsymbol{x}} \|\boldsymbol{x}\|_1 \quad \text{s.t. } \boldsymbol{Y}\boldsymbol{x} \geq 0, \|\boldsymbol{x}\|_2 = 1, \tag{4}$$

where $\boldsymbol{Y} = \text{diag}(\boldsymbol{y})\boldsymbol{A}$. Herein, $\text{diag}(\boldsymbol{y})$ returns a square diagonal matrix with the elements of vector $\boldsymbol{y}$ on the main diagonal. The ℓ_1-norm as a convex envelope of the ℓ_0-norm is a loose relaxation, thereby its solution might not be optimal [16]. To solve this issue, reweighted ℓ_1-norm as a tighter envelope is adopted as the loss function [17]. Xiao *et al.* [18] propose a Schur-concave function [19] to approximate the ℓ_0-norm and then apply it to 1-bit CS. Zhong *et al.* [20] substitute the ℓ_1-norm with the total variation semi-norm [21] for the application of image restoration. The aforementioned algorithms achieve excellent performance in noiseless environment, while their recovery accuracy might be degraded when the received signal has a small portion of sign flips caused by additive noise.

The noisy observations after quantization can be written as

$$\boldsymbol{y} = \text{sgn}(\boldsymbol{A}\boldsymbol{x} + \tilde{\boldsymbol{n}}), \tag{5}$$

where $\tilde{\boldsymbol{n}} \in \mathbb{R}^M$ is the noise vector. Extensive research has investigated the impact of thresholding or dithering on the quantization process and its subsequent effect on quantization error [22]–[24]. The dithering exhibits notable ability to reduce the overall average quantization error and facilitates a balance between accuracy and resolution. Additionally, time-varying sampling thresholds have been exploited for recovery enhancement [25]–[29].

On the other hand, under the assumption that the sparsity of the target signal is known, Jacques *et al.* [10] reformulate 1-bit CS as a fitting error minimization with sparsity and energy constraints:

$$\min_{\boldsymbol{x}} \|[\boldsymbol{y} \odot (\boldsymbol{A}\boldsymbol{x})]_-\|_p^p \quad \text{s.t. } \|\boldsymbol{x}\|_0 = S, \|\boldsymbol{x}\|_2 = 1, \tag{6}$$

where $p = 1$ or 2, $S > 0$ is the desired sparsity, and $[\boldsymbol{a}]_-$ is defined as $[\boldsymbol{a}]_- := [\min(a_1, 0), \min(a_2, 0), \ldots, \min(a_M, 0)]^\top$. The resultant problem is then addressed using iterative hard thresholding (IHT). Yan *et al.* [30] introduce an upper bound of the number of sign flips, resulting in the adaptive outlier pursuit (AOP) formulation:

$$\min_{\boldsymbol{x}, \boldsymbol{\Lambda}} \|[\boldsymbol{\Lambda} \odot \boldsymbol{y} \odot (\boldsymbol{A}\boldsymbol{x})]_-\|_2^2$$
$$\text{s.t. } \sum_{i=1}^{M} (1 - \Lambda_i) \leq L, \Lambda_i \in \{0, 1\}$$
$$\|\boldsymbol{x}\|_0 = S, \|\boldsymbol{x}\|_2 = 1, \tag{7}$$

where L is the maximum number of wrong signs, $\Lambda_i = 1$ if y_i is correct, and otherwise $\Lambda_i = 0$. When L is accurately estimated, AOP is able to attain high recovery accuracy. However, the performance of AOP will be degraded if L is inappropriately chosen. In addition, the convergence of AOP cannot be guaranteed.

Then, Fu *et al.* [31] enhance the detection approach, leading to more accurate recovery in strong noisy environment. Sivakant *et al.* [32] deal with the reconstruction task with two individual stages, namely, support restoration and approximate signal reconstruction. Fan *et al.* [33] employ ℓ_p-norm with $0 < p < 1$ to formulate the sparsity constraint, which is then converted into a penalty term. In addition, Huang and Yan [34] replace the ℓ_1-norm with minimax concave penalty and then obtain a fast algorithm with a nonconvex penalty. Dai *et al.* [35] apply maximum *a posteriori* estimation to design a robust one-sided ℓ_0-norm objective model that does not require the number of sign flips. Later, Friedlander *et al.* [36] propose the normalized binary IHT (NBIHT), whose approximation error rate matches the information-theoretic lower bound. Besides, Zhou *et al.* [11] suggest a double-sparsity constrained model:

$$\min_{\boldsymbol{x}, \boldsymbol{\Psi}} \|\boldsymbol{Y}\boldsymbol{x} + \boldsymbol{\Psi} - \alpha\boldsymbol{1}\|_2^2 + \gamma\|\boldsymbol{x}\|_2^2$$
$$\text{s.t. } \|\boldsymbol{x}\|_0 \leq S, \|[\boldsymbol{\Psi}]_+\|_0 \leq L, \tag{8}$$

where $\boldsymbol{\Psi} \in \mathbb{R}^M$, $\gamma > 0$ is the regularization parameter, and $\alpha > 0$ is a small value, such that the positive components of $(\boldsymbol{Y}\boldsymbol{x} - \alpha\boldsymbol{1})$ can be considered as the number of sign flips. Although (8) is nonconvex, gradient projection method equipped with subspace pursuit (GPSP) is able to globally converge to a unique stationary point. Nevertheless, the performance of GPSP still depends on the choice of L. Furthermore, the works [37], [38] give a linear feasibility reformulation of the 1-bit CS problem and subsequently utilize the Kaczmarz algorithm to solve the reformulation. When the cumulative distribution function (CDF) of the noise is known, [37] achieves excellent performance in the presence of erroneous signs, whereas [38] employs the upper quantile method. These two methods exhibit significantly lower computational complexity compared to other approaches. Additionally, deep unfolding has been exploited to design neural networks for 1-bit CS [39]–[42]. Specifically, [40] requires the noise CDF to achieve noise robustness, while [42] learns a surrogate value of noise covariance to enhance the signal restoration. Other works for robust 1-bit CS include , primal and dual active set (PDAS) [43], ℓ_1-norm Shannon entropy [44], and mixed 1-bit CS (M1-bit-CS) [45].

B. Motivations and Contributions

Most existing robust algorithms for 1-bit CS still face challenges from the sign flips of the measurements. A portion of them does not need the number of wrong signs, but their performance might be unsatisfactory under high noise levels. On the other hand, the algorithms that require the information of sign flips can achieve excellent restoration if the number is precisely estimated. Nevertheless, finding the flip number poses a big challenge in practice.

In this paper, we aim at devising a robust one-bit CS (ROCS) method to tackle 1-bit CS in the presence of additive noise. By remodeling the received signal after quantization, the sparsity property of quantized noise vector can be determined. We then exploit this characteristic to model the 1-bit CS

problem, which is formulated as an optimization task consisting of ℓ_2-norm and ℓ_0-norm terms, subject to the sparsity constraint on the target signal. To tackle the resultant problem, we substitute the tanh function for the sign operator and then adopt proximal alternating minimization (PAM) [46], [47] and projected gradient descent (PGD) [48] as the solver. Furthermore, theoretical properties of the suggested method, including computational complexity, as well as the convergence behavior of the loss function value and variable sequences, are provided. Our main contributions are summarized as follows:

1) *Novel observed signal model:* We remodel the quantized signal vector to investigate the characteristic of the additive noise after quantization. As the 1-bit quantizer destroys the distribution of noise, most existing signal models cannot reveal the underlying property of noise after quantization. Our new representation discloses the sparsity of the noise vector.
2) *New objective function:* Exploiting the sparsity property of the target and noise signals, we formulate the recovery problem using ℓ_2-norm and ℓ_0-norm. The former is employed to calculate the fitting error, while the latter is designed as a penalty term and constraint for sparse noise and desired signal, respectively. As a result, our approach does not require the number of sign flips.
3) *Efficient ROCS algorithm:* Although our method contains a regularization parameter, its performance is not sensitive to such a parameter. In addition, we analyze the convergence behavior of the suggested algorithm. Specifically, we show that the objective value sequence is convergent, while the variable sequence is guaranteed to converge to a critical point.
4) *Accurate estimation:* Experiment results using synthetic data demonstrate that the devised approach is superior to popular robust methodologies in noisy environments. Besides, our method is applied to DOA estimation and outperforms state-of-the-art (SOTA) algorithms.

C. Organization and Notation

The remainder of this paper is organized as follows. The proposed model and algorithm are presented in Section II. Besides, the convergence behavior and computational requirements of the algorithm are analyzed. In Section III, numerical examples are included to evaluate the devised method against several SOTA approaches. Finally, concluding remarks are given in Section IV.

Notation: The identity matrix is denoted by $\boldsymbol{I}$. The sign function for complex values is represented as $\mathrm{csgn}(\cdot)$, while the entry-wise tanh function is denoted by $\tanh_c(x) = \tanh(cx) = (e^{cx} - e^{-cx})/(e^{cx} + e^{-cx})$ with c being a positive constant. Besides, $\boldsymbol{A}^\top$ and $\boldsymbol{A}^{\mathrm{H}}$ are the transpose and Hermitian transpose of $\boldsymbol{A} \in \mathbb{R}^{M \times N}$ and $\boldsymbol{A} \in \mathbb{C}^{M \times N}$, respectively. Given a scalar a, $|a|$ is its absolute value.

II. ALGORITHM DEVELOPMENT

In this section, we present a new model for 1-bit CS and then devise an effective algorithm with convergence guarantee.

A. Proposed Model

Attempting to improve 1-bit CS in noisy environments, we model the observed signal after quantization as

$$\boldsymbol{y} = \mathrm{sgn}(\boldsymbol{A}\boldsymbol{x} + \tilde{\boldsymbol{n}}) \tag{9a}$$
$$= \mathrm{sgn}(\boldsymbol{A}\boldsymbol{x}) + \boldsymbol{n}, \tag{9b}$$

where $\boldsymbol{n} \in \mathbb{R}^M$ with $n_i \in \{-2, 0, 2\}$. In (9a), $\tilde{\boldsymbol{n}}$ is unrestricted, implying that it can represent various noise types, such as Gaussian and Laplacian noise. Even the distribution of $\tilde{\boldsymbol{n}}$ varies, the distribution of $\boldsymbol{n}$ will finally fall in the shell of the tri-valued discrete distribution because $n_i \in \{-2, 0, 2\}$, $i = 1, \ldots, N$. Nevertheless, different distributions or intensities of $\tilde{\boldsymbol{n}}$ will yield various sparsity levels of $\boldsymbol{n}$. The sparse noise is also considered in the classic CS research [49]. However, the amplitude of the sparse noise in (9b) is a deterministic constant, while that of the conventional model [49] is randomly large. Besides, [50] studies CS with the measurement matrix being corrupted by sparse errors.

We know that the recovery problem in high-bit quantization requires exploiting different norms to resist various types of distributed noise, for instance, ℓ_2-norm for Gaussian noise and ℓ_1-norm for Laplacian noise. In the context of 1-bit CS, (9b) reveals that various types of distributed noise can be transformed into the sparse noise with specific magnitudes. Consequently, we can design one formulation to resist different noise models.

For the sake of completeness, we introduce the following theorem to demonstrate the fundamental feasibility of recovering $\boldsymbol{x}$ from $\boldsymbol{y}$.

Theorem 1. *[10] Suppose that $\boldsymbol{x}^*$ with $\|\boldsymbol{x}^*\|_2 = 1$ is the ground truth, and $\bar{\boldsymbol{x}}$ is the estimate from a sparse consistent reconstruction method[1] using the measurement $\boldsymbol{y}$ corrupted by noise $\tilde{\boldsymbol{n}} \sim \mathcal{N}(0, \sigma^2)$ with $\boldsymbol{A} \sim \mathcal{N}(0, 1)^{M \times N}$, and M satisfies*

$$M \geq \frac{2}{\epsilon^2}\left(S\log(N) + 2S\log\left(\frac{35}{\epsilon}\right) + \log\left(\frac{2}{\beta}\right)\right), \tag{10}$$

where $\epsilon > 0$ is chosen to compromise between M and the upper bound of estimation error, while $0 \leq \beta \leq 1$ balances M and the probability that the estimation error is less than the upper bound. Then, we have

$$\frac{1}{\pi}\arccos\langle\bar{\boldsymbol{x}}, \boldsymbol{x}^*\rangle - \epsilon \leq \frac{1}{M}\|\mathrm{sgn}(\boldsymbol{A}\boldsymbol{x}^* + \tilde{\boldsymbol{n}}) - \mathrm{sgn}(\boldsymbol{A}\boldsymbol{x}^*)\|_0$$
$$\leq \frac{\sigma}{2} + \tau, \tag{11}$$

with a probability higher than $1 - e^{-2M\tau^2} - \beta$ where $\tau > 0$.

On the other hand, since our method handles 1-bit CS with noise, the sampling matrix must meet BϵSE [10], indicating that our method is not robust against the sampling matrix.

Based on our signal model, we formulate the recovery problem as

$$\min_{\boldsymbol{x},\boldsymbol{n}}\|\boldsymbol{y} - \mathrm{sgn}(\boldsymbol{A}\boldsymbol{x}) - \boldsymbol{n}\|_2^2 + \gamma\|\boldsymbol{n}\|_0$$
$$\text{s.t. } \|\boldsymbol{x}\|_0 \leq S, \ \|\boldsymbol{x}\|_2 = 1, \tag{12}$$

---

[1]A sparse consistent method is defined as a general nonlinear reconstruction decoder that attempts to find a solution as consistent with the measurements as possible, while guaranteeing the sparsity constraint is met [10].

where $\gamma > 0$ is a regularization parameter to control the sparsity of $\boldsymbol{n}$. Compared with most existing robust formulations that require the number of sign flips, the proposed model does not need this prior information. Moreover, in Section III, we will show that the performance of (12) is not sensitive to the selection of γ.

Furthermore, our formulation is related to adaptive least absolute shrinkage and selection operator (LASSO) [51], smoothly clipped absolute deviation (SCAD) [52], minimax-concave plus (MC+) [53], and IHT [48]. LASSO, SCAD, and MC+ yield biased estimation, whereas IHT and our formulation produce unbiased estimation. In contrast to IHT, which involves one sparse variable, our optimization problem consists of two sparse variables.

B. Proposed Algorithm

Since the sign function is discontinuous and not lower semicontinuous, it is challenging to directly tackle the resultant optimization problem (12). Therefore, we adopt the tanh function to approximate it, and their comparison is shown in Fig. 1. It is seen that c controls the degree of approximation, such that $\tanh_c(\cdot) = \text{sgn}(\cdot)$ as $c \to +\infty$. Exploiting the tanh function, we formulate the restoration task as

$$\min_{\boldsymbol{x},\boldsymbol{n}} f(\boldsymbol{x},\boldsymbol{n}) = \min_{\boldsymbol{x},\boldsymbol{n}} \|\boldsymbol{y} - \tanh_c(\boldsymbol{A}\boldsymbol{x}) - \boldsymbol{n}\|_2^2 + \gamma \|\boldsymbol{n}\|_0$$
$$\text{s.t. } \|\boldsymbol{x}\|_0 \le S. \quad (13)$$

Analogous to most existing formulations, the energy constraint is not contained in (13). After we obtain the solution, this requirement can be satisfied via normalization. As (13) involves two target variables, we exploit the PAM concept [46], [47] to address it, leading to the following iterative procedure:

$$\boldsymbol{x}^k = \arg\min_{\boldsymbol{x}, \|\boldsymbol{x}\|_0 \le S} \tilde{f}(\boldsymbol{x},\boldsymbol{n}^{k-1})$$
$$= \arg\min_{\boldsymbol{x}, \|\boldsymbol{x}\|_0 \le S} \|\boldsymbol{y} - \tanh_c(\boldsymbol{A}\boldsymbol{x}) - \boldsymbol{n}^{k-1}\|_2^2 + \mu\|\boldsymbol{x} - \boldsymbol{x}^{k-1}\|_2^2,$$
$$(14a)$$

$$\boldsymbol{n}^k = \arg\min_{\boldsymbol{n}} \tilde{f}(\boldsymbol{x}^k,\boldsymbol{n})$$
$$= \arg\min_{\boldsymbol{n}} \|\boldsymbol{y} - \tanh_c(\boldsymbol{A}\boldsymbol{x}^k) - \boldsymbol{n}\|_2^2 + \gamma\|\boldsymbol{n}\|_0$$
$$+ \mu\|\boldsymbol{n} - \boldsymbol{n}^{k-1}\|_2^2, \quad (14b)$$

where $\mu > 0$ is a pre-defined proximal parameter and the last terms in (14a) and (14b) are called proximal regularization. It is worth mentioning that μ is used for convergence guarantee, and can be set to a small value. When $\mu = 0$, PAM reduces to the classic alternating minimization [54].

As there is no closed-form solution to (14a), we adopt PGD [48] as the solver, leading to

$$\boldsymbol{x}_p^{k-1} = \mathcal{P}_\text{S}\left(\boldsymbol{x}_{p-1}^{k-1} - \eta\nabla\tilde{f}(\boldsymbol{x}_{p-1}^{k-1},\boldsymbol{n}^{k-1})\right), \quad (15)$$

where $\mathcal{P}_\text{S}(\cdot)$ is an entry-wise projection operator. Letting δ_S be the Sth largest absolute value of $(\boldsymbol{z} = \boldsymbol{x}_{p-1}^{k-1} - \eta\nabla\tilde{f}(\boldsymbol{x}_{p-1}^{k-1},\boldsymbol{n}^{k-1}))$, $\mathcal{P}_\text{S}(\boldsymbol{z})$ is defined as [55]

$$\mathcal{P}_\text{S}(z_i) = \begin{cases} z_i, & \text{if } |z_i| \ge \delta_\text{S}, \\ 0, & \text{otherwise .} \end{cases} \quad (16)$$
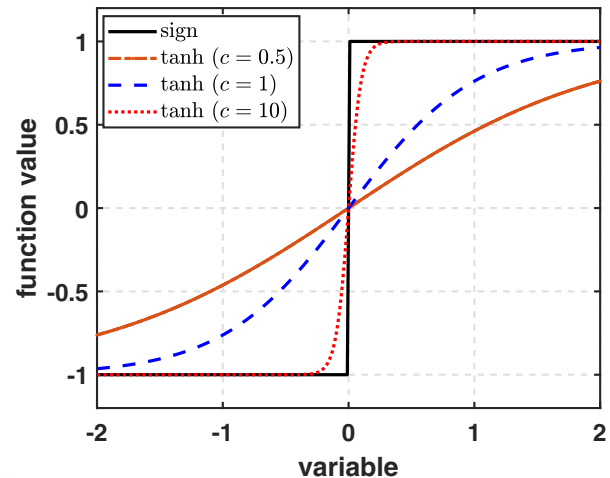

Fig. 1: Comparison of sign and tanh functions.

In addition, $\nabla\tilde{f}(\boldsymbol{x},\boldsymbol{n}^{k-1})$ is the gradient of $\tilde{f}(\boldsymbol{x},\boldsymbol{n}^{k-1})$ with respect to (w.r.t.) $\boldsymbol{x}$:

$$\nabla\tilde{f}(\boldsymbol{x},\boldsymbol{n}^{k-1})$$
$$= -2c\boldsymbol{A}^\top\left((\boldsymbol{s}^{k-1} - \tanh_c(\boldsymbol{A}\boldsymbol{x}))\odot(\boldsymbol{1} - \tanh_c(\boldsymbol{A}\boldsymbol{x})^2)\right)$$
$$+ 2\mu(\boldsymbol{x} - \boldsymbol{x}_{p-1}^{k-1}), \quad (17)$$

where $\boldsymbol{s}^{k-1} = \boldsymbol{y} - \boldsymbol{n}^{k-1}$. Herein, the superscript $(\cdot)^k$ indicates the iteration number in the PAM process, while the subscript $(\cdot)_p$ signifies the pth iteration in the PGD procedure. For the initialization of $\boldsymbol{x}_0^{k-1}$, we set $\boldsymbol{x}_0^{k-1} = \boldsymbol{x}^{k-1}$. It is worth noting that in iterative multi-variable optimization, optimizing one part to perfection while fixing remaining variables is not so beneficial [56]. This is because a perfect optimization of one part might be rendered obsolete when the other part is altered. Therefore, in practice, the iteration number to optimize $\boldsymbol{x}_p^{k-1}$ is set as $P_\text{max} = 50$, that is, $\boldsymbol{x}^k = \boldsymbol{x}_{50}^{k-1}$ is an approximate solution to (14a).

For (14b), under the definition of $\boldsymbol{e}^k = \boldsymbol{y} - \tanh_c(\boldsymbol{A}\boldsymbol{x}^k)$, it is re-expressed as

$$\boldsymbol{n}^k = \arg\min_{\boldsymbol{n}} \|\boldsymbol{e}^k - \boldsymbol{n}\|_2^2 + \gamma\|\boldsymbol{n}\|_0 + \mu\|\boldsymbol{n} - \boldsymbol{n}^{k-1}\|_2^2. \quad (18)$$

We see that n_i^k only depends on e_i^k and n_i^{k-1}, thereby (18) can be solved in an entry-wise manner:

$$n_i^k = \arg\min_{n_i} (e_i^k - n_i)^2 + \gamma|n_i|_0 + \mu(n_i - n_i^{k-1})^2. \quad (19)$$

One optimal solution to (19) is given by (see Appendix A)

$$n_i^k = \begin{cases} \frac{e_i^k + \mu n_i^{k-1}}{1+\mu}, & \gamma < (e_i^k)^2 + \mu(n_i^{k-1})^2 - \frac{\mu(n_i^{k-1} - e_i^k)^2}{1+\mu}, \\ 0, & \text{otherwise.} \end{cases} \quad (20)$$

The proposed approach is referred to as robust one-bit CS (ROCS), whose steps are summarized in Algorithm 1. Note that based on Theorem 1, ROCS cannot have a uniform recovery guarantee.

Algorithm 1 ROCS

Input: $Y \in \mathbb{R}^M$, $A \in \mathbb{R}^{M \times N}$, sparsity level S, $\mu = 10^{-8}$, $\eta = 10^{-5}$, $\gamma = 1.9^2$, $c = 10^4$, $P_{\max} = 50$, and $K_{\max} = 20$

　Initialize: Randomize $x^1 = \frac{A^\top y}{\|A^\top y\|_2}$ and $n^0 = 0$

　for $k = 1, 2, \ldots, K_{\max}$ **do**
　　　1) $x_0^{k-1} = x^{k-1}$
　　for $p = 1, \ldots, P_{\max}$ **do**
　　　　2) Update x_p^{k-1} via (15)
　　end for
　　　3) Update $x^k = x_p^{k-1}$
　　　4) Update n^k via (20)
　　　Stop if stopping criterion is met.
　end for
Output: $\frac{x^{K_{\max}}}{\|x^{K_{\max}}\|_2}$

C. Convergence Analysis

In this subsection, the convergence behavior of the proposed ROCS is analyzed. The first one exhibits the convergence of the objective values.

Theorem 2. *Let $f(x^k, n^k)$ be the objective value generated by Algorithm 1. Then, the following hold:*

(i) $\hat{f}(x) = \tilde{f}(x, n^{k-1}) + \mathcal{I}_S(x) = f(x, n^{k-1}) + \mu\|x - x_{p-1}^{k-1}\|_2^2 + \mathcal{I}_S(x)$ is a proper lower semicontinuous function with a lower bound and satisfies the KŁ property, where $\mathcal{I}_S(x)$ is an indicator function, such that $\mathcal{I}_S(x) = 0$ with $\|x\|_0 \leq S$, otherwise, $\mathcal{I}_S(x) = +\infty$. In addition, $\tilde{f}(x, n^{k-1})$ has a Lipschitz gradient.

(ii) When $0 < \eta < 1/L_{\tilde{f}}$ with $L_{\tilde{f}}$ being the Lipschitz constant of $\nabla \tilde{f}(x, n^{k-1})$ w.r.t. x, the sequence $\{f(x^k, n^k)\}_{k \in \mathbb{N}}$ is nonincreasing.

(iii) $f(x^k, n^k)$ is lower bounded.

As a result, $\{f(x^k, n^k)\}_{k \in \mathbb{N}}$ is convergent.

Proof: See Appendix B.

We then analyze the sequence behavior in Theorem 3.

Theorem 3. *Let $\{(x^k, n^k)\}_{k \in \mathbb{N}}$ be the sequence generated by Algorithm 1, where we assume that (14a) is solved exactly. Additionally, $\{(x^k, n^k)\}_{k \in \mathbb{N}}$ is considered to be bounded. Then, the following hold:*

(i)

$$\lim_{K_{\max} \to +\infty} \sum_{k=1}^{K_{\max}} (\|n^k - n^{k-1}\|_2^2 + \|x^k - x^{k-1}\|_2^2) \\ < +\infty. \qquad (21)$$

Hence, we obtain

$$\lim_{K_{\max} \to +\infty} (\|n^k - n^{k-1}\|_2 + \|x^k - x^{k-1}\|_2) = 0. \quad (22)$$

(ii) The objective function f is bounded below and has the KŁ property, and the function $(x, n) \mapsto \|y - \tanh_c(Ax) - n\|_2^2$ has a Lipschitz gradient. Then, the sequence $\{(x^k, n^k)\}_{k \in \mathbb{N}}$ converges to a critical point of (13).

(iii) The ROCS converges with at least a sublinear rate.

Proof: See Appendix C.

D. Estimation Error Bound

It is worth mentioning that one can also utilize radii of cells to obtain an upper bound for the estimation error [38], [57]. In this subsection, we exploit an alternative approach to analyze a recovery error bound of ROCS in the following lemma.

Lemma 1. *We denote x^* and x as the ground truth and its estimate, respectively. Besides, the measurement y is corrupted by noise $\tilde{n} \sim \mathcal{N}(0, \sigma^2)$ with $A \sim \mathcal{N}(0,1)^{M \times N}$, and M makes (10) hold. Then, the estimation error bound satisfies*

$$\frac{1}{\pi} \arccos\langle x, x^* \rangle \leq \frac{\bar{L}}{M} + \frac{\sigma}{2} + \tau + \epsilon, \qquad (23)$$

where $\bar{L}$ the estimated number of wrong signs.

Proof: See Appendix D.

We now analyze how $\bar{L}, M, \sigma$, and ϵ influence the recovery error bound. We consider a fixed probability of $1 - e^{-2M\tau^2} - \beta$, such that τ is a constant in (23). It is apparent that higher-intensity noise yields a larger error bound. When ϵ decreases, the error bound becomes more stringent. Since the initialized γ impacts $\bar{L}$, it also affects the error bound. Intuitively, an increase in $\bar{L}$ leads to a higher error bound. Practically, the optimal estimation performance is contingent upon the ground-truth value L^*. Consequently, the estimation accuracy does not increase monotonically as $\bar{L}$ increases from 0. That is, the trajectories of estimation performance and error bound are inconsistent with changes in $\bar{L}$.

E. Computational Complexity

In this subsection, we study the computational complexity of ROCS. The complexity of updating x^k is $\mathcal{O}(P_{\max}(MN + N\log(N)))$, where $N\log(N)$ is involved to sort $|z|$ in descending order and then determine the value of the Sth element. In addition, computing n^k has a complexity of $\mathcal{O}(MN)$. As a result, the overall computational requirement is $\mathcal{O}(K_{\max}P_{\max}(MN + N\log(N)))$.

F. Selection of γ

To facilitate investigation of γ, we set the proximal parameter μ to be 0. Consequently, we can write (20) as

$$n_i^k = \begin{cases} e_i^k, & \sqrt{\gamma} \leq |e_i^k|, \\ 0, & \text{otherwise.} \end{cases} \qquad (24)$$

As $e^k = y - \tanh_c(Ax^k)$, we have $|e_i^k| \in [0, 2]$. If $|e_i^k|$ is small, then the corresponding entry y_i can be considered to have the correct sign. When $|e_i^k| \to 2$, it indicates that y_i has been flipped. Therefore, $\sqrt{\gamma} \in (0, 2]$ can be deemed as a threshold to differentiate the correct and incorrect measurements from the fitting error. Furthermore, if c is selected as a large value, then $|e_i^k|$ tends to approach either 0 or 2. In such a case, $\sqrt{\gamma}$ should be set close to 2.
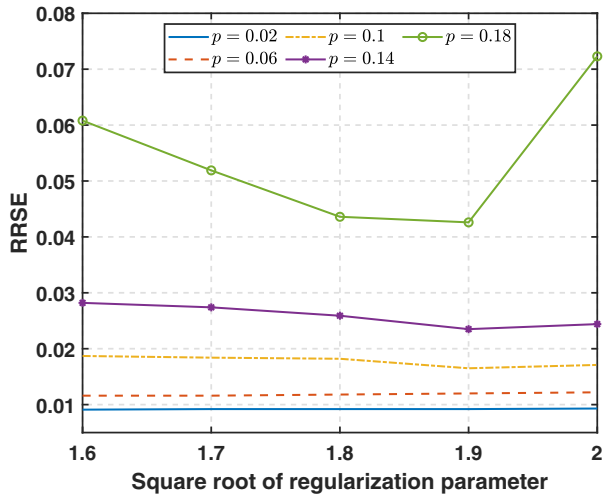
Fig. 2: RRSE versus $\sqrt{\gamma}$ in different flipping ratios.

Fig. 3: RRSE of different algorithms in 10% sign flips.

III. EXPERIMENT RESULTS

In this section, we evaluate the proposed ROCS using synthetic data and then apply it to DOA estimation. All simulations are implemented using MATLAB (R2019a) on a computer with Inter(R) Core(TM) i7- 8700 3.2GHz CPU and 16 GB memory.

A. Synthetic Data

The default settings are $M = 1000$, $N = 2000$, and $S = 5$, such that the measurement matrix is $\boldsymbol{A} \in \mathbb{R}^{1000 \times 2000}$ whose entries follow independent and identically distributed (i.i.d.) Gaussian distribution. Besides, we randomly select 5 indices from $[1, 2000]$ and then initialize their values with Gaussian distribution to obtain a sparse vector $\boldsymbol{x}^* \in \mathbb{R}^{2000}$ with normalization. Then, we get noise-free $\boldsymbol{y}^* \in \mathbb{R}^{1000}$ computed by $\text{sgn}(\boldsymbol{A}\boldsymbol{x}^*)$. As the additive noise $\boldsymbol{n}$ cannot yield a precise number of sign flips, we choose a portion of measurements at random and then flip their signs. Therefore, the noise level is measured by the ratio (denoted as p) of the number of sign flips over that of measurements. The default noise level is $p = 0.1$.

On the other hand, the recovery performance is evaluated using relative root square error (RRSE):

$$\text{RRSE} = \mathbb{E}\left\{ \frac{\|\boldsymbol{x}^* - \boldsymbol{x}\|_2}{\|\boldsymbol{x}^*\|_2} \right\} = \mathbb{E}\{\|\boldsymbol{x}^* - \boldsymbol{x}\|_2\}, \qquad (25)$$

where $\boldsymbol{x} \in \mathbb{R}^{2000}$ is the restored sparse signal and $\mathbb{E}\{\cdot\}$ denotes the mean based on 100 Monte Carlo trials. Note that a small RRSE indicates good recovery performance.

1) Investigation of γ

We have analyzed the potential values of $\sqrt{\gamma}$ in Section II. In this subsection, we study the impact of $\sqrt{\gamma}$ on recovery performance via numerical experiments. The results are plotted in Fig. 2, where the flipping ratio is selected with 5 levels. It is seen that RRSEs have little changes with $p < 0.1$, indicating that the restoration performance is not sensitive to $\sqrt{\gamma}$ when there is a small portion of sign flips. If p is large,
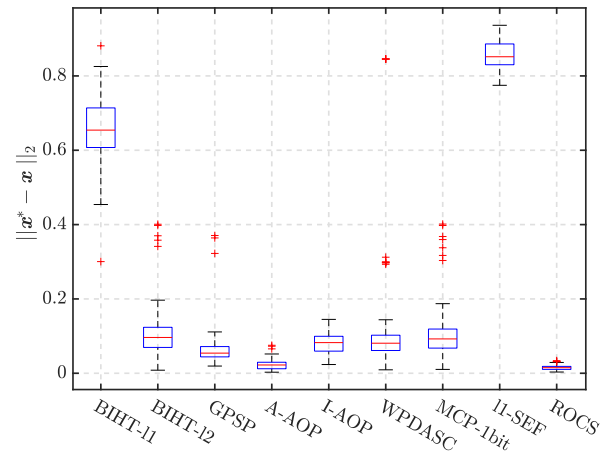
then we require an appropriate $\sqrt{\gamma}$ to differentiate the correct and incorrect measurements from the fitting error. Therefore, RRSEs change a lot as $\sqrt{\gamma}$ increases from 1.6 to 2.0, and attain the lowest value at $\sqrt{\gamma} = 1.9$. These results are consistent with our theoretical analysis.

2) Performance Comparison

We compare the ROCS with seven contemporary algorithms, namely, BIHT-ℓ_1 [10], BIHT-ℓ_2 [10], AOP [30], GPSP [11], weighted primal dual active set algorithm with continuation (WPDASC) [33], minimax concave penalty with ℓ_1-norm (MCP-ℓ_1) [34], normalized ℓ_1-Shannon entropy function (ℓ_1-SEF) [18], and learned generalized BIHT (LG-BIHT) [39]. It is worth mentioning that AOP and GPSP require the number of sign flips as their inputs. Consequently, accurate-AOP (A-AOP) indicates that AOP is given an exact pM value, while inaccurate-AOP (I-AOP) signifies that AOP has an inexact information $((p + 0.02)M)$. In addition, GPSP is provided with the exact pM.

We first compare different methods with $p = 0.1$ in Fig. 3, where the results of 100 trials are shown in a box-plot. It is seen that the restoration performance of ℓ_1-SEF and BIHT-ℓ_1 are unsatisfactory. Compared with BIHT-ℓ_2, GPSP, I-AOP, WPDASC, and MCP-1bit, A-AOP and ROCS obtain better reconstruction. We observe the performance of AOP is heavily dependent on the prior number of wrong signs. If such information is not accurate, then AOP might not attain satisfactory recovery. Furthermore, ROCS without the number of sign flips outperforms A-AOP that requires such information.

We then investigate the impact of different flipping ratios on the reconstruction performance. The results are plotted in Fig. 4, where p varies from 0 to 0.2. It is seen that the performance of ℓ_1-SEF, BIHT-ℓ_1, and LG-BIHT severely degrades as the value of p increases. When $p > 0.14$, WPDASC experiences significant performance degradation. While BIHT-ℓ_2, GPSP, AOP, MCP-1bit, and ROCS are able to attain accurate recovery under high flipping ratios. Among these algorithms, the RRSEs of the proposed method are smallest in all flipping ratios.
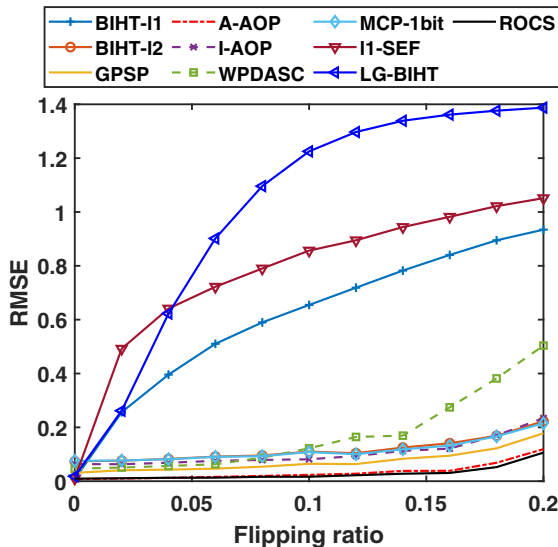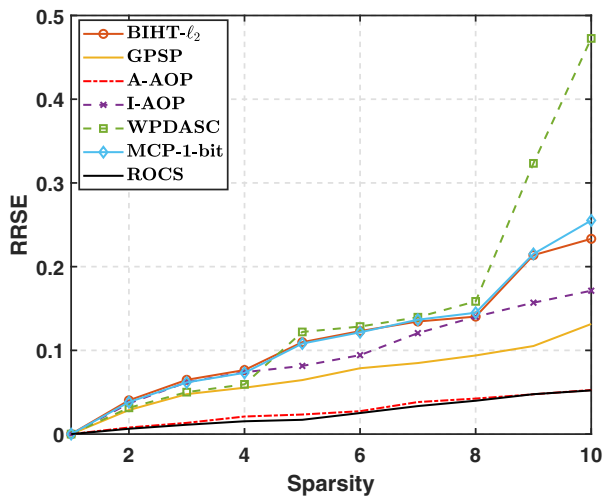
Fig. 4: RRSE versus flipping ratio.

Fig. 5: RRSE versus sparsity in 10% sign flips.

Fig. 6: RRSE versus measurement number with 10% sign flips.

Besides, the effect of sparsity on the restoration is studied in Fig. 5, where the sparsity covers $[1, 10]$. The results of ℓ_1-SEF, BIHT-ℓ_1, and LG-BIHT are not shown as their RRSEs are very large, which is not conducive to distinguish the performance of other algorithms. It is observed that RRSEs of all methods increase with the sparsity level. Among these seven approaches, ROCS and AOP with accurate pM value are superior to BIHT-ℓ_2, GPSP, I-AOP, WPDASC, and MCP-1-bit. Compared with A-AOP, ROCS shows a little advantage.

Furthermore, we compare the recovery performance of different approaches when the measurement number varies from 800 to 1600. The results are shown in Fig. 6 with $p = 0.1$ and $S = 5$. It is observed that ROCS shows remarkable superiority over its competitors.

B. Direction-of-Arrival Estimation

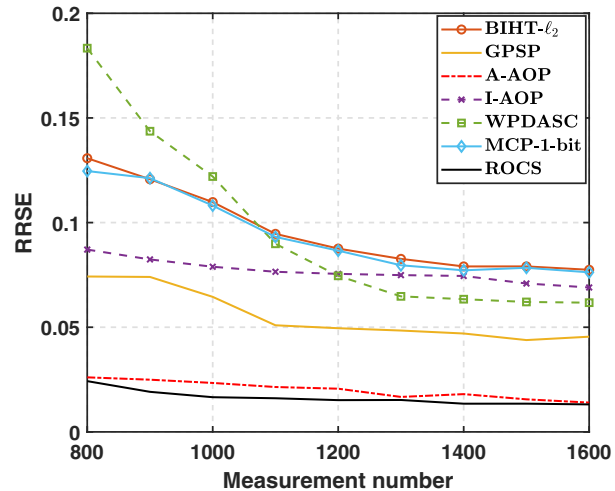A well-known application of 1-bit CS is DOA estimation and we apply ROCS to this task.

In the pioneering work [58], Bar–Shalom and Weiss have addressed this issue and proposed reconstructing the unquantized (original) covariance matrix based on the arcsine law. This reconstruction scheme has been subsequently utilized for DOA estimation in sparse arrays [59], [60]. Furthermore, [61] derives a conservative approximation of the corresponding Cramér-Rao bound. Additionally, extensive works focus on covariance recovery [62]–[66] and then the estimated covariance matrix can be exploited for DOA estimation. Furthermore, one-bit Hankel matrix completion has been applied to DOA estimation [67].

1) Problem Formulation

Consider a uniform linear array (ULA) equipped with M sensors, where the spacing between adjacent sensors is d. It is essential that the spacing satisfies $d \leq \lambda/2$ in order to avoid phase ambiguity, where λ is the wavelength of the incoming signal. Assume S far-field, uncorrelated narrow-band signals are impinging upon the array from distinct directions $\boldsymbol{\theta} = [\theta_1, \theta_2, \ldots, \theta_S]^\top$. The discrete-time complex-valued base-band signal received by the mth sensor at time instant q is modeled as [68]

$$\widetilde{y}_m(q) = \sum_{s=1}^{S} x_s(q) e^{\text{j}2\pi(m-1)\sin(\theta_s)\frac{d}{\lambda}} + n_m(q), \qquad (26)$$

where $x_s(q)$ denotes the sth source signal, $\text{j} = \sqrt{-1}$ is the imaginary unit, and $n_m(q)$ represents the additive noise.

Organizing the output signal of the M sensors into the vector form, we have

$$\widetilde{\boldsymbol{y}}_q = \boldsymbol{A}\boldsymbol{x}_q + \boldsymbol{n}_q, \qquad (27)$$

where $\widetilde{\boldsymbol{y}}_q = [\widetilde{y}_1(q), \ldots, \widetilde{y}_M(q)]^\top \in \mathbb{C}^M$ is the received signal vector, $\boldsymbol{x}_q = [x_1(q), \ldots, x_S(q)]^\top \in \mathbb{C}^S$ is the source vector, $\boldsymbol{n}_q = [n_1(q), \ldots, n_M(q)]^\top \in \mathbb{C}^M$ is the noise vector, and $\boldsymbol{A} \in \mathbb{C}^{M \times S}$ is the array manifold matrix

$$\boldsymbol{A} = [\boldsymbol{a}(\theta_1), \ldots, \boldsymbol{a}(\theta_S)]. \qquad (28)$$

with $\boldsymbol{a}(\theta_s)$ being the steering vector given by

$$\boldsymbol{a}(\theta_s) = \left[1, e^{\mathrm{j}2\pi \sin(\theta_s)\frac{d}{\lambda}}, \ldots, e^{\mathrm{j}2\pi(M-1)\sin(\theta_s)\frac{d}{\lambda}}\right]^\top. \quad (29)$$

Collecting Q snapshots, the received signal is represented as

$$\begin{aligned}
\widetilde{\boldsymbol{Y}} &= [\widetilde{\boldsymbol{y}}_1, \ldots, \widetilde{\boldsymbol{y}}_Q] \\
&= \boldsymbol{AX} + \boldsymbol{N}. \quad (30)
\end{aligned}$$

where $\boldsymbol{X} = [\boldsymbol{x}_1, \boldsymbol{x}_2, \ldots, \boldsymbol{x}_Q] \in \mathbb{C}^{S \times Q}$ and $\boldsymbol{N} = [\boldsymbol{n}_1, \boldsymbol{n}_2, \ldots, \boldsymbol{n}_Q] \in \mathbb{C}^{M \times Q}$. Then, the quantized signal with 1-bit ADC is expressed as

$$\boldsymbol{Y} = \mathrm{csgn}(\widetilde{\boldsymbol{Y}}) = \mathrm{sgn}(\Re(\widetilde{\boldsymbol{Y}})) + \mathrm{jsgn}(\Im(\widetilde{\boldsymbol{Y}})), \quad (31)$$

where $\Re(\cdot)$ and $\Im(\cdot)$ are the real and imaginary parts of a complex number, respectively.

To find $\boldsymbol{\theta}$, we discretize the potential DOA range (i.e. $[-90°, 90°]$) into $\bar{S}$ grids:

$$\boldsymbol{\theta} \subset \bar{\boldsymbol{\theta}} = [\bar{\theta}_1, \bar{\theta}_2, \ldots, \bar{\theta}_{\bar{S}}]^\top, \quad (32)$$

where $\bar{\boldsymbol{\theta}}$ is not quantized. It is worth pointing out that the quantization of $\bar{\boldsymbol{\theta}}$ is able to improve transmission process [69]. Then, the quantized signal is re-expressed as

$$\boldsymbol{Y} = \mathrm{csgn}(\bar{\boldsymbol{A}}\bar{\boldsymbol{X}} + \boldsymbol{N}), \quad (33)$$

where $\bar{\boldsymbol{A}} \in \mathbb{C}^{M \times \bar{S}}$ is the extended array manifold

$$\bar{\boldsymbol{A}} = [\boldsymbol{a}(\bar{\theta}_1), \ldots, \boldsymbol{a}(\bar{\theta}_{\bar{S}})] \quad (34)$$

and $\bar{\boldsymbol{X}} \in \mathbb{C}^{\bar{S} \times Q}$ is the extended signal matrix, which is a row-sparse matrix. Specifically, its ith row equals the jth row of $\boldsymbol{X}$ if $\bar{\theta}_i = \theta_j$. Furthermore, the quantized signal (33) can be rewritten into the real-valued form [70]

$$\boldsymbol{Y}_r = \mathrm{sgn}(\bar{\boldsymbol{A}}_r \bar{\boldsymbol{X}}_r + \boldsymbol{N}_r), \quad (35)$$

where

$$\boldsymbol{Y}_r = [\Re(\boldsymbol{Y}); \Im(\boldsymbol{Y})], \quad (36a)$$
$$\bar{\boldsymbol{A}}_r = [\Re(\bar{\boldsymbol{A}}), -\Im(\bar{\boldsymbol{A}}); \Im(\bar{\boldsymbol{A}}), \Re(\bar{\boldsymbol{A}})], \quad (36b)$$
$$\bar{\boldsymbol{X}}_r = [\Re(\bar{\boldsymbol{X}}); \Im(\bar{\boldsymbol{X}})], \quad (36c)$$
$$\boldsymbol{N}_r = [\Re(\boldsymbol{N}); \Im(\boldsymbol{N})]. \quad (36d)$$

The DOAs can be estimated from

$$\min_{\bar{\boldsymbol{X}}_r, \boldsymbol{N}_r} \|\boldsymbol{Y}_r - \tanh_c(\bar{\boldsymbol{A}}_r \bar{\boldsymbol{X}}_r) - \boldsymbol{N}_r\|_F^2 + \gamma \|\boldsymbol{N}_r\|_0$$
$$\text{s.t. } \|\bar{\boldsymbol{X}}\|_{2,0} \leq S, \quad (37)$$

where $\|\bar{\boldsymbol{X}}\|_{2,0} = \|[\sum_{j=1}^Q x_{1,j}^2, \sum_{j=1}^Q x_{2,j}^2, \ldots, \sum_{j=1}^Q x_{\bar{S},j}^2]^\top\|_0$ is the $\ell_{2,0}$-norm. It is worth mentioning that the sparsity constraint is implemented on the complex-valued $\bar{\boldsymbol{X}}$. Besides, the normalization does not impact the result of DOA estimation and thus the energy constraint is omitted in (37). For the $\ell_{2,0}$-norm constraint, we first compute the ℓ_2-norm of each row of $\bar{\boldsymbol{X}}$ to obtain a vector that is the spatial frequency spectrum. We then retain the first S largest peaks, and set the other entries to 0.

2) Simulation Setting

Unless stated otherwise, the signals are Gaussian distributed with equal power, and the ULA is comprised of $M = 20$
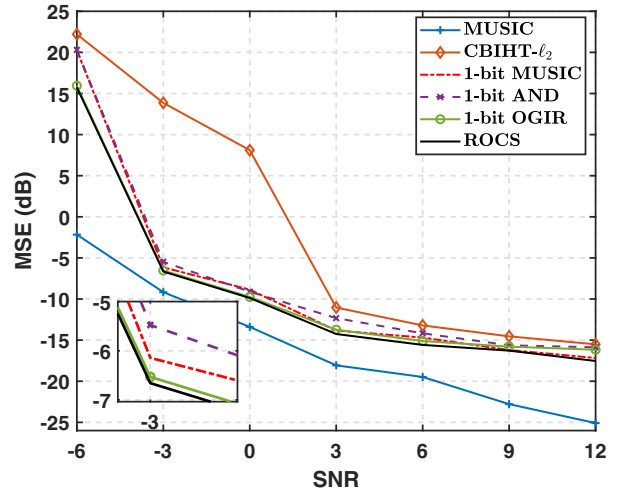

Fig. 7: MSE versus SNR in zero-mean white Gaussian noise.
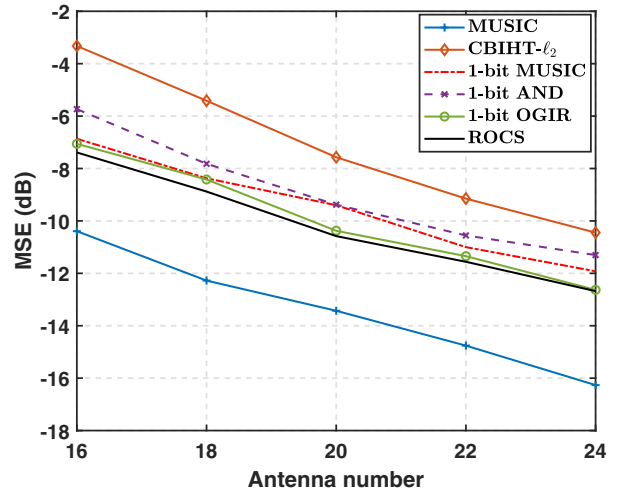
Fig. 8: MSE versus antenna number at SNR = 0dB.

sensors with the inter-element spacing of $d = 0.5\lambda$. Besides, the number of snapshots is $Q = 32$, and the DOAs of three signals are $\theta_1 = -30°$, $\theta_2 = 5°$, and $\theta_3 = 20°$. In addition, we add the zero-mean white Gaussian noise into the clean signal, and the signal-to-noise ratio (SNR) is defined as

$$\mathrm{SNR} = 10\log_{10}\left(\frac{\|\boldsymbol{AX}\|_F^2}{\sigma^2}\right), \quad (38)$$

where σ^2 is the noise variance. Furthermore, the estimation performance is measured by the mean square error (MSE) in dB, which is defined as

$$\mathrm{MSE} = 10\log_{10}\left(\frac{1}{M_c}\sum_{m=1}^{M_c}\sum_{s=1}^{S}\frac{(\widehat{\theta}_{s,m} - \theta_s)^2}{S}\right). \quad (39)$$

Here, $M_c = 100$ is the number of Monte Carlo trials and $\widehat{\theta}_{s,m}$ is the sth DOA estimate at the mth trial.

3) Performance Comparison

The proposed method is compared with five popular algorithms, namely, multiple signal classification (MUSIC) [71],

Fig. 9: MSE versus target number at SNR = 0dB.

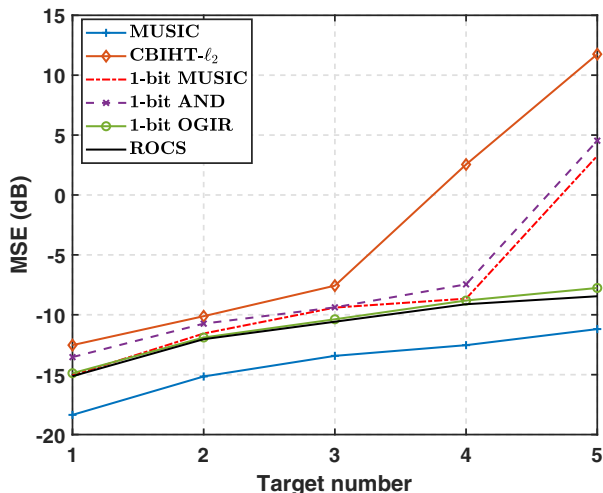1-bit MUSIC [68], complex-valued BIHT based on ℓ_2-norm (CBIHT-ℓ_2) [70], 1-bit atomic norm denoising (1-bit AND) [72], and 1-bit-off-grid iterative reweighted (1-bit OGIR) [73]. Herein, the results of MUSIC depend on the unquantized measurements.

We first evaluate all algorithms under different SNRs, and the results are plotted in Fig. 7. We see that MUSIC attains smallest MSEs in all SNRs since its received signal does not have the quantization error. ROCS and 1-bit OGIR attain comparable estimation performance in low SNRs, while ROCS outperforms 1-bit OGIR in high SNRs. Overall, ROCS exhibits superiority over other 1-bit algorithms.

The performance of six methods under different numbers of antennas is investigated in Fig. 8 at SNR = 0dB. It is observed that MUSIC still attains the best performance, while ROCS yields smaller MSEs than other 1-bit algorithms.

Furthermore, we compare all methods with different numbers of targets. The results are shown in Fig. 9, where the DOAs of the fourth and fifth signals are $\theta_4 = -15°$ and $\theta_5 = 30°$. When the target number increases, the estimation performance of 1-bit MUSIC, CBIHT-ℓ_2, and 1-bit AND seriously degrades, while MUSIC, 1-bit OGIR, and ROCS still achieve satisfactory performance for 5 targets. Among the 1-bit algorithms, ROCS attains the lowest MSEs as target number varies from 1 to 5.

IV. CONCLUSION

In this article, we reformulated the quantized measurement model for 1-bit CS, such that the sparsity property of the noise vector after quantization can be utilized to enhance restoration. We then formulated the corresponding optimization problem using ℓ_2-norm and ℓ_0-norm, where the former is exploited to restrict the fitting error, while the latter is designed as a penalty term and constraint for sparse noise and desired signal, respectively. Besides, we adopted proximal alternating minimization and projected gradient descent to tackle the resultant optimization task. Although the proposed ROCS has an auxiliary parameter γ, its performance is not sensitive to

γ. We analyzed the practical significance of γ. Specifically, its square root can be considered as a threshold to differentiate the correct and incorrect signs in the received signal. We also analyzed convergence behavior of ROCS. Specifically, we showed that the objective value sequence is convergent, while the variable sequence converges to a critical point. Simulation results demonstrated that ROCS achieves better performance than popular algorithms in terms of recovery accuracy with sign flips. ROCS was also applied to DOA estimation and was shown to outperform the SOTA methods based on 1-bit quantization.

As our future works, we will extend the proposed robust approach in other applications of 1-bit signal processing, including phase retrieval [74], quadratic CS [75], high dynamic range imaging [76], and so on.

APPENDIX A
DERIVATION OF SOLUTION TO (19)

To find the solution to (19), we discuss the following two cases:

(i) For $n_i = 0$, the minimum objective function value is $(e_i^k)^2 + \mu(n_i^{k-1})^2$

(ii) For $n_i \neq 0$, the minimizer is $n_i = \frac{e_i^k + \mu n_i^{k-1}}{1+\mu}$ and the corresponding function value is

$$\inf_{n_i}\{(e_i^k - n_i)^2 + \lambda|n_i|_0 + \mu(n_i - n_i^{k-1})^2\}$$
$$= \frac{\mu(n_i^{k-1} - e_i^k)^2}{1+\mu} + \lambda. \qquad (40)$$

When this minimum is less than that with $n_i = 0$, the solution to (19) should be $n_i^k = \frac{e_i^k + \mu n_i^{k-1}}{1+\mu}$, otherwise, $n_i^k = 0$. To summarize, we have

$$n_i^k = \begin{cases} \frac{e_i^k + \mu n_i^{k-1}}{1+\mu}, & \lambda \leq (e_i^k)^2 + \mu(n_i^{k-1})^2 - \frac{\mu(n_i^{k-1} - e_i^k)^2}{1+\mu} \\ 0, & \text{otherwise.} \end{cases} \qquad (41)$$

Note that both $n_i^k = \frac{e_i^k + \mu n_i^{k-1}}{1+\mu}$ and $n_i^k = 0$ are the optimal solution when $\lambda = (e_i^k)^2 + \mu(n_i^{k-1})^2 - \frac{\mu(n_i^{k-1} - e_i^k)^2}{1+\mu}$. Since n_i^k is independent of n_j^k for $i \neq j$, the optimal solution of each element results in optimal $\boldsymbol{n}^k$ to (19). The proof is complete. ∎

APPENDIX B
PROOF OF THEOREM 2

A. Property (i)

We have

$$\hat{f}(\boldsymbol{x}) = \tilde{f}(\boldsymbol{x}, \boldsymbol{n}^{k-1}) + \mathcal{I}_S(\boldsymbol{x}) \qquad (42a)$$
$$= \|\boldsymbol{y} - \tanh_c(\boldsymbol{Ax}) - \boldsymbol{n}^{k-1}\|_2^2 + \mu\|\boldsymbol{x} - \boldsymbol{x}_{p-1}^{k-1}\|_2^2 + \mathcal{I}_S(\boldsymbol{x}), \qquad (42b)$$

It is clear that $\hat{f}$ is lower semicontinuous and lower bounded. Besides, it is known that $\tanh_c(\cdot)$ function is definable in an o-minimal structure [46], and $\|\boldsymbol{x}\|_0 \leq S$ is a nonempty closed semi-algebraic set [77]. Therefore, $\tilde{f}(\boldsymbol{x})$ is definable in an o-minimal structure, implying that it has the KŁ property [46].

Then, we prove that $\tilde{f}(\cdot, \boldsymbol{n}^{k-1})$ has a Lipschitz gradient. Its first and second derivatives are

$$\nabla_{\boldsymbol{x}} f(\boldsymbol{x}, \boldsymbol{n}^{k-1}) = -2c\boldsymbol{A}^{\top}\Big((\boldsymbol{s}-\tanh_c(\boldsymbol{Ax}))\odot(\boldsymbol{1}-\tanh_c(\boldsymbol{Ax})^2)\Big)$$
$$+ 2\mu(\boldsymbol{x}-\boldsymbol{x}_{p-1}^{k-1}), \tag{43a}$$
$$\nabla_{\boldsymbol{x}}^2 f(\boldsymbol{x}, \boldsymbol{n}^{k-1}) = 2c^2(\boldsymbol{D}_1\boldsymbol{A})^{\top}\boldsymbol{A}+4c^2(\boldsymbol{D}_2\boldsymbol{A})'\boldsymbol{A}+2\mu\boldsymbol{I}, \tag{43b}$$

where $\boldsymbol{s} = \boldsymbol{y} - \boldsymbol{n}^{k-1}$, $\boldsymbol{D}_1 = \operatorname{diag}\Big((\boldsymbol{1} - \tanh_c(\boldsymbol{Ax})^2) \odot (\boldsymbol{1} - \tanh_c(\boldsymbol{Ax})^2)\Big)$, and $\boldsymbol{D}_2 = \operatorname{diag}\Big((\boldsymbol{s} - \tanh_c(\boldsymbol{Ax})) \odot \tanh_c(\boldsymbol{Ax}) \odot (\boldsymbol{1} - \tanh_c(\boldsymbol{Ax})^2)\Big)$. As $-1 \leq \tanh_c(\boldsymbol{a}_{i,:}\boldsymbol{x}) \leq 1$ for $i \in [1, M]$, we obtain

$$|\tanh_c(\boldsymbol{a}_{i,:}\boldsymbol{x})(1 - \tanh_c(\boldsymbol{a}_{i,:}\boldsymbol{x})^2)| < \frac{1}{2}, \tag{44a}$$
$$\|\boldsymbol{D}_1\|_2 \leq 1, \tag{44b}$$
$$\|\boldsymbol{D}_2\|_2 \leq \frac{1}{2}\|\operatorname{diag}(\boldsymbol{s} - \tanh_c(\boldsymbol{Ax}))\|_2$$
$$\leq \frac{1}{2}(\|\operatorname{diag}(\boldsymbol{s})\|_2 + \|\operatorname{diag}(-\tanh_c(\boldsymbol{Ax}))\|_2)$$
$$\leq \frac{1}{2}(1 + 1) = 1. \tag{44c}$$

Moreover, we get

$$\|\nabla_{\boldsymbol{x}}^2 f(\boldsymbol{x}, \boldsymbol{n}^{k-1})\|_2$$
$$= \|2c^2(\boldsymbol{D}_1\boldsymbol{A})^{\top}\boldsymbol{A} + 4c^2(\boldsymbol{D}_2\boldsymbol{A})^{\top}\boldsymbol{A} + 2\mu\boldsymbol{I}\|_2 \tag{45a}$$
$$\leq 2c^2\|(\boldsymbol{D}_1\boldsymbol{A})^{\top}\boldsymbol{A}\|_2 + 4c^2\|(\boldsymbol{D}_2\boldsymbol{A})^{\top}\boldsymbol{A}\|_2 + 2\mu \tag{45b}$$
$$\leq 2c^2\|\boldsymbol{D}_1\|_2\|\boldsymbol{A}\|_2^2 + 4c^2\|\boldsymbol{D}_2\|_2\|\boldsymbol{A}\|_2^2 + 2\mu \tag{45c}$$
$$\leq 6c^2\|\boldsymbol{A}\|_2^2 + 2\mu. \tag{45d}$$

When $\|\boldsymbol{A}\|_F$ is finite, $\|\boldsymbol{A}\|_2^2 \leq \|\boldsymbol{A}\|_F^2 < +\infty$ must hold, resulting in $6c^2\|\boldsymbol{A}\|_2^2 + 2\mu < +\infty$. As a result, the function $\tilde{f}(\cdot, \boldsymbol{n}^{k-1})$ has a Lipschitz gradient. The proof is complete. ∎

B. Property (ii)

For (14a), it is equivalent to

$$\min_{\boldsymbol{x}} \hat{f}(\boldsymbol{x}). \tag{46}$$

Since (46) is solved using (15) and thus based on [77], we have

$$\hat{f}(\boldsymbol{x}_p^{k-1}) - \hat{f}(\boldsymbol{x}_{p-1}^{k-1}) \leq -\frac{a_{\tilde{f}}}{2}\|\boldsymbol{x}_p^{k-1} - \boldsymbol{x}_{p-1}^{k-1}\|_2^2, \tag{47}$$

where $a_{\tilde{f}} > 6c^2\|\boldsymbol{A}\|_2^2 + 2\mu$.

By induction on p, we further obtain

$$\hat{f}(\boldsymbol{x}^k) - \hat{f}(\boldsymbol{x}^{k-1}) \leq \sum_{p=1}^{P_{\max}} -\frac{a_{\tilde{f}}}{2}\|\boldsymbol{x}_p^{k-1} - \boldsymbol{x}_{p-1}^{k-1}\|_2^2 \tag{48a}$$
$$\Leftrightarrow f(\boldsymbol{x}^k, \boldsymbol{n}^{k-1}) - f(\boldsymbol{x}^{k-1}, \boldsymbol{n}^{k-1})$$
$$\leq -\mu\|\boldsymbol{x}^k - \boldsymbol{x}^{k-1}\|_2^2 - \sum_{p=1}^{P_{\max}}\frac{a_{\tilde{f}}}{2}\|\boldsymbol{x}_p^{k-1} - \boldsymbol{x}_{p-1}^{k-1}\|_2^2, \tag{48b}$$

where $\mu > 0$, $\boldsymbol{x}_0^{k-1} = \boldsymbol{x}^{k-1}$ and $\boldsymbol{x}^k = \boldsymbol{x}_{P_{\max}}^{k-1}$. We see that updating $\boldsymbol{x}$ does not increase the objective value.

On the other hand, as (20) seeks one optimal solution of (14b), we have

$$\|\boldsymbol{y} - \tanh_c(\boldsymbol{Ax}^k) - \boldsymbol{n}^k\|_2^2 + \lambda\|\boldsymbol{n}^k\|_0 + \mu\|\boldsymbol{n}^k - \boldsymbol{n}^{k-1}\|_2^2$$
$$\leq \|\boldsymbol{y} - \tanh_c(\boldsymbol{Ax}^k) - \boldsymbol{n}^{k-1}\|_2^2 + \lambda\|\boldsymbol{n}^{k-1}\|_0 \tag{49a}$$
$$\Leftrightarrow f(\boldsymbol{x}^k, \boldsymbol{n}^k) - f(\boldsymbol{x}^k, \boldsymbol{n}^{k-1}) \leq -\mu\|\boldsymbol{n}^k - \boldsymbol{n}^{k-1}\|_2^2. \tag{49b}$$

Combining (48b) and (49b) results in

$$f(\boldsymbol{x}^k, \boldsymbol{n}^k) - f(\boldsymbol{x}^{k-1}, \boldsymbol{n}^{k-1}) \leq 0, \tag{50}$$

which indicates that $f(\boldsymbol{x}^k, \boldsymbol{n}^k)$ is nonincreasing after updating the variables. The proof is complete. ∎

C. Property (iii)

Since $f(\boldsymbol{x}, \boldsymbol{n})$ is comprised of two terms based on ℓ_2-norm and ℓ_0-norm, respectively, $f(\boldsymbol{x}^k, \boldsymbol{n}^k) \geq 0$ must hold.

As a result, based on Properties (ii) and (iii), the convergence of $\{f(\boldsymbol{x}^k, \boldsymbol{n}^k)\}_{k\in\mathbb{N}}$ is guaranteed. The proof is complete. ∎

APPENDIX C
PROOF OF THEOREM 3

A. Property (i)

From (48b), we get

$$f(\boldsymbol{x}^{k-1}, \boldsymbol{n}^{k-1}) - f(\boldsymbol{x}^k, \boldsymbol{n}^{k-1}) \geq \mu\|\boldsymbol{x}^k - \boldsymbol{x}^{k-1}\|_2^2. \tag{51}$$

Combining (51) and (49b) yields

$$\|\boldsymbol{n}^k - \boldsymbol{n}^{k-1}\|_2^2 + \|\boldsymbol{x}^k - \boldsymbol{x}^{k-1}\|_2^2$$
$$\leq \frac{f(\boldsymbol{x}^{k-1}, \boldsymbol{n}^{k-1}) - f(\boldsymbol{x}^k, \boldsymbol{n}^k)}{\mu}. \tag{52}$$

By induction on k, we obtain

$$\lim_{K_{\max}\to+\infty} \sum_{k=1}^{K_{\max}} (\|\boldsymbol{n}^k - \boldsymbol{n}^{k-1}\|_2^2 + \|\boldsymbol{x}^k - \boldsymbol{x}^{k-1}\|_2^2)$$
$$\leq \lim_{K_{\max}\to+\infty} \frac{f(\boldsymbol{x}^0, \boldsymbol{n}^0) - f(\boldsymbol{x}^{K_{\max}}, \boldsymbol{n}^{K_{\max}})}{\mu}$$
$$< +\infty. \tag{53}$$

Therefore, under the assumption that $\{(\boldsymbol{x}^k, \boldsymbol{n}^k)\}_{k\in\mathbb{N}}$ is bounded, we have

$$\lim_{K_{\max}\to+\infty}(\|\boldsymbol{n}^k - \boldsymbol{n}^{k-1}\|_2 + \|\boldsymbol{x}^k - \boldsymbol{x}^{k-1}\|_2) = 0. \tag{54}$$

The proof is complete. ∎

B. Property (ii)

It is obvious that f is bounded below. In addition, as the ℓ_0-norm is semi-algebraic, it is also definable in an o-minimal structure [78]. Combining Property (i) in Appendix B, we conclude that f has the KŁ property.

On the other hand, we have proved the following function has a Lipschitz gradient:

$$\tilde{f}(\boldsymbol{x}, \boldsymbol{n}^{k-1}) = \|\boldsymbol{y} - \tanh_c(\boldsymbol{Ax}) - \boldsymbol{n}^{k-1}\|_2^2 + \mu\|\boldsymbol{x} - \boldsymbol{x}_{p-1}^{k-1}\|_2^2. \tag{55}$$

Therefore, the function $(\boldsymbol{x}, \boldsymbol{n}) \mapsto \|\boldsymbol{y} - \tanh_c(\boldsymbol{A}\boldsymbol{x}) - \boldsymbol{n}\|_2^2$ has a Lipschitz gradient w.r.t. $\boldsymbol{x}$. We then prove that it has a Lipschitz gradient w.r.t. $\boldsymbol{n}$:

$$\left\|\frac{\partial^2 \|\boldsymbol{y} - \tanh_c(\boldsymbol{A}\boldsymbol{x}) - \boldsymbol{n}\|_2^2}{\partial^2 \boldsymbol{n}}\right\|_2 = \|2\boldsymbol{I}\|_2 \le 2, \ \forall \boldsymbol{n} \in \mathbb{R}^M. \quad (56)$$

As a result, the function $(\boldsymbol{x}, \boldsymbol{n}) \mapsto \|\boldsymbol{y} - \tanh_c(\boldsymbol{A}\boldsymbol{x}) - \boldsymbol{n}\|_2^2$ has a Lipschitz gradient.

Furthermore, as $\min_{\boldsymbol{x}, \boldsymbol{n}} f(\boldsymbol{x}, \boldsymbol{n})$ is solved using PAM and $(\boldsymbol{x}^k, \boldsymbol{n}^k)_{k \in \mathbb{N}}$ is bounded, $\{(\boldsymbol{x}^k, \boldsymbol{n}^k)\}_{k \in \mathbb{N}}$ converges to a critical point of (13) based on Theorem 6.2 in [77]. The proof is complete. ∎

C. Property (iii)

As f has the KŁ property, based on Theorem 1 in [78], our method converges at least sublinearly. The proof is complete. ∎

APPENDIX D
PROOF OF LEMMA 1

Prior to analyzing the upper error bound of ROCS, we introduce the following lemma.

Lemma 2. *Given two vectors* $\boldsymbol{a} \in \mathbb{R}^M$ *and* $\boldsymbol{b} \in \mathbb{R}^M$, *we have*

$$\|\boldsymbol{a} + \boldsymbol{b}\|_0 \le \|\boldsymbol{a}\|_0 + \|\boldsymbol{b}\|_0. \quad (57)$$

Proof: We assume that $\|\boldsymbol{a}\|_0 = S_1$ with $\Phi_1 = \{a_i | a_i \ne 0\}$, and $\|\boldsymbol{b}\|_0 = S_2$ with $\Phi_2 = \{b_i | b_i \ne 0\}$. Then, we discuss the following two cases:

(i) $S_1 + S_2 < M$: When $\Phi_1 \cap \Phi_2 = \phi$, $\|\boldsymbol{a} + \boldsymbol{b}\|_0$ reaches its maximum at $S_1 + S_2$, thereby satisfying the equality condition.

(ii) $S_1 + S_2 \ge M$: It is apparent that the largest value of $\|\boldsymbol{a} + \boldsymbol{b}\|_0$ is M, which meets the inequality condition. ∎

Let $\tilde{\boldsymbol{y}} = \boldsymbol{y} - \boldsymbol{n}$ in the recovery problem (12). Then, $\tilde{\boldsymbol{y}}$ can be considered as the measurement without noise corruption and thus the proposed method aims at seeking a solution that not only achieves consistency with the denoised measurement but also satisfies the sparsity condition. Therefore, based on (11) in Theorem 1, we have

$$\frac{1}{M}\|\mathrm{sgn}(\boldsymbol{A}\boldsymbol{x}^* + \tilde{\boldsymbol{n}}) - \mathrm{sgn}(\boldsymbol{A}\boldsymbol{x}^*)\|_0 \le \frac{\sigma}{2} + \tau. \quad (58)$$

Besides, according to the bounded angle error [10], we obtain

$$\frac{1}{\pi}\arccos\langle\bar{\boldsymbol{x}}, \boldsymbol{x}^*\rangle \le \frac{1}{M}\|\mathrm{sgn}(\boldsymbol{A}\bar{\boldsymbol{x}}) - \mathrm{sgn}(\boldsymbol{A}\boldsymbol{x}^*)\|_0 + \epsilon \quad (59a)$$

$$\le \frac{1}{M}(\|\mathrm{sgn}(\boldsymbol{A}\bar{\boldsymbol{x}}) - \mathrm{sgn}(\boldsymbol{A}\boldsymbol{x}^* + \bar{\boldsymbol{n}})\|_0 + \|\mathrm{sgn}(\boldsymbol{A}\boldsymbol{x}^* + \bar{\boldsymbol{n}}) - \mathrm{sgn}(\boldsymbol{A}\boldsymbol{x}^*)\|_0) + \epsilon \quad (59b)$$

$$\le \frac{1}{M}\|\mathrm{sgn}(\boldsymbol{A}\bar{\boldsymbol{x}}) - \mathrm{sgn}(\boldsymbol{A}\boldsymbol{x}^* + \bar{\boldsymbol{n}})\|_0 + \frac{\sigma}{2} + \tau + \epsilon \quad (59c)$$

$$\le \frac{1}{M}(\|\mathrm{sgn}(\boldsymbol{A}\bar{\boldsymbol{x}}) - \boldsymbol{y}\|_0 + \|\boldsymbol{y} - \mathrm{sgn}(\boldsymbol{A}\boldsymbol{x}^* + \bar{\boldsymbol{n}})\|_0) + \frac{\sigma}{2} + \tau + \epsilon \quad (59d)$$

$$= \frac{1}{M}\|\mathrm{sgn}(\boldsymbol{A}\bar{\boldsymbol{x}}) - \boldsymbol{y}\|_0 + \frac{\sigma}{2} + \tau + \epsilon. \quad (59e)$$

Additionally, we consider a special situation in which γ gradually approaches 0 for a sufficient number of iterations. Let us review (20):

$$n_i^k = \begin{cases} \frac{e_i^k + \mu n_i^{k-1}}{1 + \mu}, & \gamma < (e_i^k)^2 + \mu(n_i^{k-1})^2 - \frac{\mu(n_i^{k-1} - e_i^k)^2}{1 + \mu}, \\ 0, & \text{otherwise.} \end{cases} \quad (60)$$

When $\gamma \to 0$ and $\mu \to 0$, we have

$$\|\mathrm{sgn}(\boldsymbol{A}\bar{\boldsymbol{x}}) - \boldsymbol{y}\|_0 = \|\boldsymbol{n}\|_0. \quad (61)$$

That is, $\|\mathrm{sgn}(\boldsymbol{A}\bar{\boldsymbol{x}}) - \boldsymbol{y}\|_0$ equals the estimated number of wrong signs, denoted as $\bar{L}$. Since our optimization problem is nonconvex, the value of $\bar{L}$ is affected by the initialized value of γ. Consequently, we obtain

$$\frac{1}{\pi}\arccos\langle\bar{\boldsymbol{x}}, \boldsymbol{x}^*\rangle \le \frac{\bar{L}}{M} + \frac{\sigma}{2} + \tau + \epsilon. \quad (62)$$

The proof is complete. ∎

REFERENCES

[1] D. L. Donoho, "Compressed sensing," *IEEE Trans. Inf. Theory*, vol. 52, no. 4, pp. 1289–1306, Apr. 2006.

[2] E. J. Candès and M. B. Wakin, "An introduction to compressive sampling," *IEEE Signal Process. Mag.*, vol. 25, no. 2, pp. 21–30, Mar. 2008.

[3] P. T. Boufounos and R. G. Baraniuk, "1-bit compressive sensing," in *Proc. 42nd Annu. Conf. Inf. Sci. Syst.*, Princeton, NJ, USA, Mar. 2008, pp. 16–21.

[4] B. Zhao, L. Huang, J. Li, M. Liu, and J. Wang, "Deceptive SAR jamming based on 1-bit sampling and time-varying thresholds," *IEEE J. Sel. Topics Appl. Earth Observ. Remote Sens.*, vol. 11, no. 3, pp. 939–950, Feb. 2018.

[5] B. Zhao, L. Huang, and W. Bao, "One-bit SAR imaging based on single-frequency thresholds," *IEEE Trans. Geosci. Remote Sens.*, vol. 57, no. 9, pp. 7017–7032, Apr. 2019.

[6] P. Xiao, B. Liao, and N. Deligiannis, "DeepFPC: A deep unfolded network for sparse signal recovery from 1-bit measurements with application to DOA estimation," *Signal Process.*, vol. 176, p. 107699, Nov. 2020.

[7] M. Chen, Q. Li, X. P. Li, L. Huang, and M. Rihan, "One-bit doa estimation for deterministic signals based on $\ell_{2,1}$-norm minimization," *IEEE Trans. Aerosp. Electron. Syst.*, Jan. 2024, (Early Access), DOI: 10.1109/TAES.2023.3348084.

[8] C.-H. Chen and J.-Y. Wu, "Amplitude-aided 1-bit compressive sensing over noisy wireless sensor networks," *IEEE Wireless Commun. Lett.*, vol. 4, no. 5, pp. 473–476, Jun. 2015.

[9] B. Sun and Y. Ni, "A training-free one-bit compressed sensing framework for wireless neural recording," *IEEE Commun. Lett.*, vol. 21, no. 8, pp. 1775–1778, 2017.

[10] L. Jacques, J. N. Laska, P. T. Boufounos, and R. G. Baraniuk, "Robust 1-bit compressive sensing via binary stable embeddings of sparse vectors," *IEEE Trans. Inf. Theory*, vol. 59, no. 4, pp. 2082–2102, Apr. 2013.

[11] S. Zhou, Z. Luo, N. Xiu, and G. Y. Li, "Computing one-bit compressive sensing via double-sparsity constrained optimization," *IEEE Trans. Signal Process.*, vol. 70, pp. 1593–1608, Mar. 2022.

[12] K. Knudson, R. Saab, and R. Ward, "One-bit compressive sensing with norm estimation," *IEEE Trans. Inf. Theory*, vol. 62, no. 5, pp. 2748–2758, May 2016.

[13] A. Ameri, A. Bose, J. Li, and M. Soltanalian, "One-bit radar processing with time-varying sampling thresholds," *IEEE Trans. Signal Process.*, vol. 67, no. 20, pp. 5297–5308, Sep. 2019.

[14] C. Xu and L. Jacques, "Quantized compressive sensing with RIP matrices: The benefit of dithering," *Inf. Inference: A J. IMA*, vol. 9, no. 3, pp. 543–586, 2020.

[15] L. Vandenberghe and S. Boyd, "Semidefinite programming," *SIAM Rev.*, vol. 38, no. 1, pp. 49–95, Mar. 1996.

[16] X. P. Li, Z.-L. Shi, C.-S. Leung, and H. C. So, "Sparse index tracking with k-sparsity or ε-deviation constraint via ℓ_0-norm minimization," *IEEE Trans. Neural Netw. Learn. Syst.*, vol. 34, no. 12, pp. 10930–10943, Dec. 2022.

This article has been accepted for publication in IEEE Transactions on Signal Processing. This is the author's version which has not been fully edited and content may change prior to final publication. Citation information: DOI 10.1109/TSP.2024.3387346

10th-April-2024

[17] H. Wang, X. Huang, Y. Liu, S. Van Huffel, and Q. Wan, "Binary reweighted ℓ_1-norm minimization for one-bit compressed sensing," in *Proc. 8th Int. Joint Conf. Biomed. Eng. Syst. Technol.*, Lisbon, Portugal, Jan. 2015, pp. 206–210.

[18] P. Xiao, B. Liao, and J. Li, "One-bit compressive sensing via Schur-concave function minimization," *IEEE Trans. Signal Process.*, vol. 67, no. 16, pp. 4139–4151, Aug. 2019.

[19] K. Kreutz-Delgado and B. D. Rao, "A general approach to sparse basis selection: Majorization, concavity, and affine scaling," Univ. Calif, SanDiego, CA, USA, Tech. Rep., 1997.

[20] Y. Zhong, C. Xu, B. Zhang, J. Hou, and J. Wang, "One-bit compressed sensing via total variation minimization method," *Signal Process.*, vol. 207, p. 108939, Jun. 2023.

[21] D. Needell and R. Ward, "Stable image reconstruction using total variation minimization," *SIAM J. Imaging Sci.*, vol. 6, no. 2, pp. 1035–1058, Jun. 2013.

[22] R. G. Baraniuk, S. Foucart, D. Needell, Y. Plan, and M. Wootters, "Exponential decay of reconstruction error from binary measurements of sparse signals," *IEEE Trans. Inf. Theory*, vol. 63, no. 6, pp. 3368–3385, Jun. 2017.

[23] A. Eamaz, F. Yeganegi, and M. Soltanalian, "Matrix completion from one-bit dither samples," *arXiv:2310.03224*, 2023.

[24] ——, "Matrix completion via memoryless scalar quantization," *arXiv:2311.05052*, 2023.

[25] A. Eamaz, K. V. Mishra, F. Yeganegi, and M. Soltanalian, "UNO: Unlimited sampling meets one-bit quantization," *IEEE Trans. Signal Process.*, vol. 72, no. 2, pp. 997–1014, Jan. 2024.

[26] A. Eamaz, F. Yeganegi, D. Needell, and M. Soltanalian, "ORKA: Accelerated Kaczmarz algorithms for signal recovery from one-bit samples," *arXiv:2301.03467*, 2022.

[27] A. Eamaz, F. Yeganegi, and M. Soltanalian, "One-bit matrix completion with time-varying sampling thresholds," in *Poc. Int. Confe. Sampling Theory and Applications*, New Haven, CT, USA, Jul. 2023, pp. 1–5.

[28] F. Yeganegi, A. Eamaz, and M. Soltanalian, "Low-rank matrix sensing with dithered one-bit quantization," *arXiv:2309.04045*, 2023.

[29] A. Eamaz, K. V. Mishra, F. Yeganegi, and M. Soltanalian, "Unlimited sampling via one-bit quantization," in *Proc. Int. Conf. Sampling Theory Appl.*, New Haven, CT, USA, Nov. 2023, pp. 1–5.

[30] M. Yan, Y. Yang, and S. Osher, "Robust 1-bit compressive sensing using adaptive outlier pursuit," *IEEE Trans. Signal Process.*, vol. 60, no. 7, pp. 3868–3875, Jul. 2012.

[31] X. Fu, F.-M. Han, and H. Zou, "Robust 1-bit compressive sensing against sign flips," in *Proc. Glob. Commun. Conf.*, Austin, TX, USA, Dec. 2014, pp. 3121–3125.

[32] S. Gopi, P. Netrapalli, P. Jain, and A. Nori, "One-bit compressed sensing: Provable support and vector recovery," in *Proc. Int. Conf. Mach. Learn.*, Atlanta, Georgia, USA, Jun. 2013, pp. 154–162.

[33] Q. Fan, C. Jia, J. Liu, and Y. Luo, "Robust recovery in 1-bit compressive sensing via ℓ_p-constrained least squares," *Signal Process.*, vol. 179, p. 107822, Feb. 2021.

[34] X. Huang and M. Yan, "Nonconvex penalties with analytical solutions for one-bit compressive sensing," *Signal Process.*, vol. 144, pp. 341–351, Oct. 2018.

[35] D.-Q. Dai, L. Shen, Y. Xu, and N. Zhang, "Noisy 1-bit compressive sensing: Models and algorithms," *Appl. Comput. Harmon. Anal.*, vol. 40, no. 1, pp. 1–32, Jan. 2016.

[36] M. P. Friedlander, H. Jeong, Y. Plan, and Ö. Yılmaz, "NBIHT: An efficient algorithm for 1-bit compressed sensing with optimal error decay rate," *IEEE Trans. Inf. Theory*, vol. 68, no. 2, pp. 1157–1177, Nov. 2021.

[37] A. Eamaz, F. Yeganegi, and M. Soltanalian, "One-bit phase retrieval: More samples means less complexity?" *IEEE Trans. Signal Process.*, vol. 70, pp. 4618–4632, Sep. 2022.

[38] A. Eamaz, F. Yeganegi, D. Needell, and M. Soltanalian, "Harnessing the power of sample abundance: Theoretical guarantees and algorithms for accelerated one-bit sensing," *arXiv:2308.00695*, 2023.

[39] S. Khobahi and M. Soltanalian, "Model-based deep learning for one-bit compressive sensing," *IEEE Trans. Signal Process.*, vol. 68, pp. 5292–5307, Sep. 2020.

[40] S. Khobahi, N. Naimipour, M. Soltanalian, and Y. C. Eldar, "Deep signal recovery with one-bit quantization," in *Proc. IEEE Int. Conf. Acoust. Speech Signal Process.*, Brighton, UK, May 2019, pp. 2987–2991.

[41] Y. Zeng, S. Khobahi, and M. Soltanalian, "One-bit compressive sensing: Can we go deep and blind?" *IEEE Signal Process Lett.*, vol. 29, pp. 1629–1633, Jun. 2022.

[42] S. Khobahi, N. Shlezinger, M. Soltanalian, and Y. C. Eldar, "LoRD-Net: Unfolded deep detection network with low-resolution receivers," *IEEE Trans. Signal Process.*, vol. 69, pp. 5651–5664, Oct. 2021.

[43] J. Huang, Y. Jiao, X. Lu, and L. Zhu, "Robust decoding from 1-bit compressive sampling with ordinary and regularized least squares," *SIAM J. Sci. Comput.*, vol. 40, no. 4, pp. A2062–A2086, Jan. 2018.

[44] P. Xiao and B. Liao, "Robust one-bit compressive sensing with weighted ℓ_1-norm minimization," *Signal Processing*, vol. 164, pp. 380–385, Jun. 2019.

[45] X. Huang, H. Yang, Y. Huang, L. Shi, F. He, A. Maier, and M. Yan, "Robust mixed one-bit compressive sensing," *Signal Process.*, vol. 162, pp. 161–168, Sep. 2019.

[46] H. Attouch, J. Bolte, P. Redont, and A. Soubeyran, "Proximal alternating minimization and projection methods for nonconvex problems: An approach based on the Kurdyka-Łojasiewicz inequality," *Math. Oper. Res.*, vol. 35, no. 2, pp. 438–457, Apr. 2010.

[47] F. Wen, R. Ying, P. Liu, and T.-K. Truong, "Nonconvex regularized robust PCA using the proximal block coordinate descent algorithm," *IEEE Trans. Signal Process.*, vol. 67, no. 20, pp. 5402–5416, Oct. 2019.

[48] T. Blumensath and M. E. Davies, "Iterative thresholding for sparse approximations," *J. Fourier Anal. Appl.*, vol. 14, pp. 629–654, Sep. 2008.

[49] J. N. Laska, M. A. Davenport, and R. G. Baraniuk, "Exact signal recovery from sparsely corrupted measurements through the pursuit of justice," in *Proc. Conf. Rec. 43rd Asilomar Conf. Signals Syst. Comput.*, Pacific Grove, CA, USA, Nov. 2009, pp. 1556–1560.

[50] Y. Chen, C. Caramanis, and S. Mannor, "Robust sparse regression under adversarial corruption," in *Proc. Int. Conf. Mach. Learn.*, Princeton, NJ, USA, Jun. 2013, pp. 774–782.

[51] R. Tibshirani, "Regression shrinkage and selection via the LASSO," *J. Roy.Stat. Soc., Ser. B, Methodol.*, vol. 58, no. 1, pp. 267–288, Mar. 1996.

[52] J. Fan and R. Li, "Variable selection via nonconcave penalized likelihood and its oracle properties," *J. Amer. Statist. Assoc.*, vol. 96, no. 456, pp. 1348–1360, Dec. 2001.

[53] C.-H. Zhang, "Nearly unbiased variable selection under minimax concave penalty," 2010.

[54] A. Beck, "On the convergence of alternating minimization for convex programming with applications to iteratively reweighted least squares and decomposition schemes," *SIAM J. Optim.*, vol. 25, no. 1, pp. 185–209, Jan. 2015.

[55] X. P. Li, Z.-L. Shi, Q. Liu, and H. C. So, "Fast robust matrix completion via entry-wise ℓ_0-norm minimization," *IEEE Trans. Cybern.*, vol. 53, no. 11, pp. 7199–7212, Nov. 2023.

[56] Q. Liu and X. Li, "Efficient low-rank matrix factorization based on $\ell_{1,\varepsilon}$-norm for online background subtraction," *IEEE Trans. Circuits Syst. Video Technol.*, vol. 32, no. 7, pp. 4900–4904, Jul. 2021.

[57] E. Lybrand, A. Ma, and R. Saab, "On the number of faces and radii of cells induced by gaussian spherical tessellations," *Appl. Comput. Harmon. A.*, vol. 56, pp. 176–188, Jan. 2022.

[58] O. Bar-Shalom and A. J. Weiss, "DOA estimation using one-bit quantized measurements," *IEEE Trans. Aerosp. Electron. Syst.*, vol. 38, no. 3, pp. 868–884, Jun. 2002.

[59] C.-L. Liu and P. Vaidyanathan, "One-bit sparse array DOA estimation," in *Proc. IEEE Int. Conf. Acoust. Speech Signal Process.*, New Orleans, LA, USA, May 2017, pp. 3126–3130.

[60] S. Sedighi, B. Shankar, M. Soltanalian, and B. Ottersten, "One-bit DoA estimation via sparse linear arrays," in *Proc. IEEE Int. Conf. Acoust. Speech Signal Process.*, Barcelona, Spain, Apr. 2020, pp. 9135–9139.

[61] S. Sedighi, M. Soltanalian, and B. Ottersten, "On the performance of one-bit DOA estimation via sparse linear arrays," *IEEE Trans. Signal Process.*, vol. 69, pp. 6165–6182, Oct. 2021.

[62] A. Eamaz, F. Yeganegi, and M. Soltanalian, "Covariance recovery for one-bit sampled stationary signals with time-varying sampling thresholds," *Signal Process.*, vol. 206, p. 108899, May 2023.

[63] ——, "Covariance recovery for one-bit sampled non-stationary signals with time-varying sampling thresholds," *IEEE Trans. Signal Process.*, vol. 70, pp. 5222–5236, Oct. 2022.

[64] ——, "Modified arcsine law for one-bit sampled stationary signals with time-varying thresholds," in *Proc. IEEE Int. Conf. Acoust., Speech Signal Process.*, Toronto, ON, Canada, Jun. 2021, pp. 5459–5463.

[65] T. Yang, J. Maly, S. Dirksen, and G. Caire, "Plug-in channel estimation with dithered quantized signals in spatially non-stationary massive MIMO systems," *arXiv:2301.04641*, 2023.

[66] S. Dirksen, J. Maly, and H. Rauhut, "Covariance estimation under one-bit quantization," *Ann. Statist.*, vol. 50, no. 6, pp. 3538–3562, Dec. 2022.

[67] A. Eamaz, F. Yeganegi, Y. Hu, S. Sun, and M. Soltanalian, "Automotive radar sensing with sparse linear arrays using one-bit Hankel matrix completion," *arXiv:2312.05423*, 2023.

[68] X. Huang and B. Liao, "One-bit MUSIC," *IEEE Signal Process. Lett.*, vol. 26, no. 7, pp. 961–965, Jul. 2019.

This article has been accepted for publication in IEEE Transactions on Signal Processing. This is the author's version which has not been fully edited and content may change prior to final publication. Citation information: DOI 10.1109/TSP.2024.3387346

10ᵗʰ-April-2024

13

[69] Z. Esmaeilbeig, A. Eamaz, K. V. Mishra, and M. Soltanalian, "Quantized phase-shift design of active IRS for integrated sensing and communications," in *Proc. IEEE Int. Conf. Acoust., Speech, Signal Process. Workshops (ICASSPW)*, Rhodes Island, Greece, Aug. 2023, pp. 1–5.

[70] P. Wang, H. Yang, and Z. Ye, "1-bit direction of arrival estimation via improved complex-valued binary iterative hard thresholding," *Digital Signal Process.*, vol. 120, p. 103265, Oct. 2022.

[71] R. Schmidt, "Multiple emitter location and signal parameter estimation," *IEEE Trans. Antennas Propag.*, vol. 34, no. 3, pp. 276–280, Mar. 1986.

[72] Z. Wei, W. Wang, F. Dong, and Q. Liu, "Gridless one-bit direction-of-arrival estimation via atomic norm denoising," *IEEE Commun. Lett.*, vol. 24, no. 10, pp. 2177–2181, Jun. 2020.

[73] L. Feng, L. Huang, Q. Li, Z.-Q. He, and M. Chen, "An off-grid iterative reweighted approach to one-bit direction of arrival estimation," *IEEE Trans. Veh. Technol.*, vol. 72, no. 6, pp. 8134–8139, Jun. 2023.

[74] A. Eamaz, F. Yeganegi, and M. Soltanalian, "OPeRA: Leveraging the sample size and complexity trade-off towards efficient one-bit phase retrieval," in *Proc. 56th Asilomar Conf. Signals, Syst., Comput.*, Pacific Grove, CA, USA, Oct. 2022, pp. 81–85.

[75] A. Eamaz, F. Yeganegi, D. Needell, and M. Soltanalian, "One-bit quadratic compressed sensing: From sample abundance to linear feasibility," in *Proc. IEEE Int. Symp. Inf. Theory (ISIT)*, Taipei, Taiwan, Aug. 2023, pp. 1154–1159.

[76] A. Eamaz, F. Yeganegi, and M. Soltanalian, "HDR imaging with one-bit quantization," *arXiv:2309.03982*, 2023.

[77] H. Attouch, J. Bolte, and B. F. Svaiter, "Convergence of descent methods for semi-algebraic and tame problems: Proximal algorithms, forward–backward splitting, and regularized Gauss–Seidel methods," *Math. Program.*, vol. 137, no. 1-2, pp. 91–129, Aug. 2013.

[78] J. Bolte, S. Sabach, and M. Teboulle, "Proximal alternating linearized minimization for nonconvex and nonsmooth problems," *Math. Programming*, vol. 146, no. 1-2, pp. 459–494, Jul. 2014.

Lei Huang (M'07-SM'14) received the B. Sc. and Ph. D. degrees in electronic engineering from Xidian University, Xi'an, China, in 2000 and 2005, respectively. He is currently with the College of Electronics and Information Engineering, Shenzhen University, as a Chair Professor, and established the Shenzhen Key Laboratory of Advanced Navigation Technology (ANT) as the Founding Director. He is now the Executive Dean of the College of Electronics and Information Engineering and the Executive Director of the State Key Laboratory of Radio Frequency Heterogeneous Integration, Shenzhen University. Dr. Huang's research interests include spectral estimation, array signal processing, statistical signal processing, and their applications in radar, navigation and wireless communications. In these areas, he has published 130 IEEE journal papers, and undertaken 20 national and provincial key projects, such as the Key Project of the National Natural Science Foundation of China (NSFC) and Joint Project of NSFC-RGC (Hong Kong). He was the winner of the Distinguished Young Scientists of NSFC. Dr. Huang severed as a Senior Area Editor of IEEE Transactions on Signal Processing (2019-2023), and an Associate Editor of IEEE Transactions on Signal Processing (2015-2019). He also was on the editorial boards of Elsevier-Digital Signal Processing (2012-2019) and has been on the editorial boards of IET Signal Processing (2017-present), and an elected member of Sensor Array and Multichannel (SAM) Technical Committee of the IEEE Signal Processing Society (2016-2022).

Xiao-Peng Li (M'23) received the B.Eng. degree as an outstanding graduate in Electronic Science and Technology from Yanshan University, Qinhuangdao, China, in 2015, and the M.Sc. degree with Distinction in Electronic Information Engineering and the Ph.D. degree in Electrical Engineering from the City University of Hong Kong, Hong Kong SAR, China, in 2018 and 2022, respectively. He was a Research Assistant with the Department of Information Engineering, Shenzhen University, Shenzhen, China from 2018 to 2019, and a Postdoctoral Fellow with the Department of Electrical Engineering, City University of Hong Kong from 2022 to 2023. He is currently an Assistant Professor with the College of Electronics and Information Engineering, Shenzhen University. His research interests include robust signal processing, sparse recovery, matrix processing, tensor processing, optimization methods, machine learning, and their applications in various areas of engineering, including target estimation, image recovery, video restoration, hyperspectral unmixing, and stock market analysis.
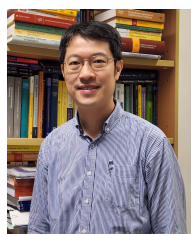
Anthony Man-Cho So (Fellow, IEEE) received the B.S.E. degree in computer science from Princeton University, Princeton, NJ, USA, with minors in applied and computational mathematics, engineering and management systems, and German language and culture; the M.Sc. degree in computer science and the Ph.D. degree in computer science with a Ph.D. minor in mathematics from Stanford University, Stanford, CA, USA. He is currently Dean of the Graduate School, Deputy Master of Morningside College, and a Professor with the Department of Systems Engineering and Engineering Management at The Chinese University of Hong Kong (CUHK), Hong Kong SAR, China. His research interests include optimization theory and its applications in various areas of science and engineering, including computational geometry, machine learning, signal processing, and statistics.

Dr. So has been a Fellow of IEEE since 2023 and an Outstanding Fellow of the Faculty of Engineering at CUHK since 2019. He is the recipient of a number of research and teaching awards, including the SIAM Review SIGEST Award in 2024, the 2022 University Grants Committee (UGC) Teaching Award, the 2018 IEEE Signal Processing Society Best Paper Award, the 2015 IEEE Signal Processing Society Signal Processing Magazine Best Paper Award, the 2014 IEEE Communications Society Asia-Pacific Outstanding Paper Award, the 2013 CUHK Vice-Chancellor's Exemplary Teaching Award, and the 2010 INFORMS Optimization Society Optimization Prize for Young Researchers. He currently serves on the Editorial Boards of *Journal of Global Optimization*, *Mathematics of Operations Research*, *Mathematical Programming*, *Open Journal of Mathematical Optimization*, *Optimization Methods and Software*, and *SIAM Journal on Optimization*. He was also the Lead Guest Editor of the Special Issue on Non-Convex Optimization for Signal Processing and Machine Learning of the IEEE SIGNAL PROCESSING MAGAZINE.

Zhang-Lei Shi received the Ph.D. degree from the Department of Electrical Engineering, City University of Hong Kong, Hong Kong SAR, China, in 2021. He is currently a Lecturer with the College of Science, China University of Petroleum (East China), Qingdao, China. His current research interests include neural networks, machine learning, and sparse optimization.

Hing Cheung So (S'90–M'95–SM'07-F'15) was born in Hong Kong. He received the B.Eng. degree from the City University of Hong Kong and the Ph.D. degree from The Chinese University of Hong Kong, both in electronic engineering, in 1990 and 1995, respectively. From 1990 to 1991, he was an Electronic Engineer with the Research and Development Division, Everex Systems Engineering Ltd., Hong Kong. During 1995–1996, he was a Postdoctoral Fellow with The Chinese University of Hong Kong. From 1996 to 1999, he was a Research Assistant Professor with the Department of Electronic Engineering, City University of Hong Kong, where he is currently a Professor. His research interests include detection and estimation, fast and adaptive algorithms, multidimensional harmonic retrieval, robust signal processing, source localization, and sparse approximation.

He has been on the editorial boards of *IEEE Signal Processing Magazine* (2014–2017), *IEEE Transactions on Signal Processing* (2010–2014), *Signal Processing* (2010–), and *Digital Signal Processing* (2011–). He was also Lead Guest Editor for *IEEE Journal of Selected Topics in Signal Processing*, special issue on "Advances in Time/Frequency Modulated Array Signal Processing" in 2017. In addition, he was an elected member in Signal Processing Theory and Methods Technical Committee (2011–2016) of the IEEE Signal Processing Society where he was chair in the awards subcommittee (2015–2016).